Tuning Mechanism through Buffer Dependence of Hydrogen Evolution Catalyzed by a Cobalt Mini-enzyme

*Jennifer M. Le[a], Georgios Alachouzos[a], Alison J. Frontier[a], Angela Lombardi[b], Kara L. Bren[a]**

[a]*Department of Chemistry, University of Rochester, Rochester, NY 14627, USA*

[b]*Department of Chemical Sciences, University of Naples Federico II, Complesso Universitario Monte S. Angelo, via Cintia 45, 80126 Naples, Italy*

Corresponding author:

Kara L. Bren
Email: bren@chem.rochester.edu
Address: Department of Chemistry, University of Rochester, Rochester, NY 14627, USA
Phone number: (585) 275-4335

TOC GRAPHIC

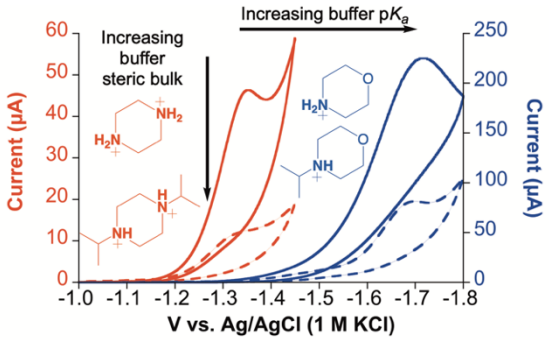

ABSTRACT: Cobalt-mimochrome VI*a (CoMC6*a) is a synthetic mini-protein that catalyzes aqueous proton reduction to hydrogen (H_2). In buffered water, there are multiple possible proton donors, complicating the elucidation of mechanism. We have found that buffer pK_a and sterics have significant effects on activity, evaluated through cyclic voltammetry (CV). Protonated buffer is proposed to act as the primary proton donor to the catalyst, specifically through the protonated amine of the buffers that were tested. At a constant pH of 6.5, catalytic H_2 evolution in the presence of buffer acids of pK_a ranging from 5.8 to 11.6 was investigated, giving rise to a potential-pK_a relationship that can be divided into two regions. For acids of p$K_a \leq 8.7$, the half-wave catalytic potential (E_h) changes as a function of pK_a with a slope of –128 mV/pK_a unit, and for acids of p$K_a \geq 8.7$, E_h changes as a function of pK_a with a slope of –39 mV/pK_a unit. In addition, a series of buffer acids was synthesized to explore the influence of steric bulk around the acidic proton on catalysis. The catalytic current in CV shows a significant decrease in the presence of the sterically hindered buffer acids compared to their parent compounds, also consistent with the added buffer acid acting as the primary proton donor to the catalyst and showing that acid structure in addition to pK_a impacts activity. These results demonstrate that buffer acidity and structure are important considerations when optimizing and evaluating systems for proton-dependent catalysis in water.

Introduction

In the context of providing a sustainable and renewable energy carrier, hydrogen (H_2) would ideally be derived from water. Advancements in the development of H_2-evolution catalysts include synthetic catalysts that operate in 100% water[1–7] and/or the introduction of proton transfer pathways that yield more efficient catalysts.[8–11] Further developments in the field require mechanistic investigations of proton transfer to the catalyst in water. There is precedent for the role of buffer in mediating proton transfers in a heterogeneous polycrystalline Au electrode system for proton reduction,[12] homogenous electrocatalytic systems for water oxidation,[13–17] and a homogenous electrocatalytic and photocatalytic system for CO_2 reduction using nickel cyclam.[18] In the case of the heterogenous system for proton reduction, preassociation of the buffer in the electrochemical double layer plays a role in interfacial proton transfer.[12] In the homogenous electrocatalytic systems for water oxidation, buffer is proposed to play multiple roles including acting as a base in proton abstraction from water,[13–17] inhibiting catalysis through anation,[13,16] and/or facilitating a proton-coupled electron transfer step leading to O–O bond formation.[13–16] In the CO_2 reduction system, the activity and selectivity for CO_2 reduction is impacted by association of the buffer with the catalyst.[18] A classic example in enzyme kinetics involves the buffer role in proton abstraction to regenerate the basic form of the catalytically active zinc site in carbonic anhydrase for interaction with CO_2.[19] As demonstrated by these examples, it is evident that the buffer is not always innocent when evaluating systems in water. Here, we report our findings that buffer structure and pK_a both play roles in determining H_2-evolution activity and mechanism for the mini-protein catalyst CoMC6*a.

The CoMC6*a scaffold consists of a cobalt deuteroporphyrin covalently bound to a distal decapeptide chain and a proximal tetradecapeptide chain through peptide lysine chains condensed with deuteroporphyrin propionic acid moieties, where the tetradecapeptide chain provides an axial His to the cobalt ion (Figure 1). CoMC6*a was previously reported to electrocatalytically reduce protons to H_2 in pH 6.5 buffered water with a turnover number (TON) of 230,000.[2] The overpotential for H_2 evolution was observed to be lowered as a function of increased peptide folding of CoMC6*a by up to 90 mV.[2] In addition, electrochemical characterization in dimethylformamide (DMF) supports the hypothesis that a Co(I) species must be accessed for catalysis to occur when using acetic acid as the proton source (pK_a value of ~13.5 in DMF[20]).[2] Cobalt-catalyzed H_2 evolution by a single-site, metal-centered mechanism typically invokes the formation of a cobalt-hydride by protonation of a low-valent cobalt species.[21–23]

During the catalytic cycle, two electrons and two protons are assembled through proposed

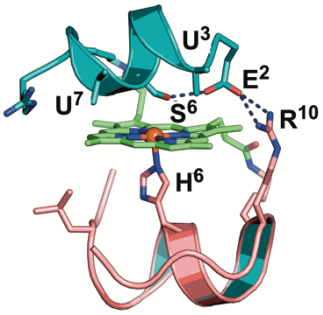

Figure 1. A model of CoMC6*a (ref. 2). CoMC6*a is a mini-protein consisting of a distal decapeptide and proximal tetradecapeptide, each of which is covalently attached to a cobalt deuteroporphyrin through an amide bond between a peptide lysine side chain and porphyrin propionic acid moiety. Selected labeled residues are represented as sticks.

pathways that involve protonation of Co(I) to form a Co(III)-hydride, which is protonated to yield H_2 either directly or after a subsequent reduction step.[22] Mechanistic studies of cobalt H_2-evolution catalysts conducted in organic solvent suggest that strong acids are required for H_2 evolution by protonating the Co(III)-H species,[23,24] whereas weak acids are competent to protonate the Co(II)-H species. [24–26] Homolytic pathways involving H_2 formation by bimolecular reactions of Co(III)-H or Co(II)-H also are possible[27] but will not be invoked in this work, as concentrations of the buffer conjugate acid used here are in excess relative to catalyst. Furthermore, the structure of CoMC6*a, in which the cobalt porphyrin is protected by peptides on both faces, is expected to inhibit catalyst-catalyst interactions (Figure 1).

The solubility and reactivity of this mini-protein in water near neutral pH is particularly notable, as the preponderance of known H_2-evolution catalysts function in organic solvent with added organic acids or in mixtures with water, while relatively few function in water[22,23,28] especially near neutral pH[1,2,29–31] despite the significant interest in developing H_2-evolution catalysis in water.[32–34] Here, we report potential-pK_a relationships for H_2-evolution catalysis by CoMC6*a in the presence of various buffer acids in water, giving insight into the possible mechanisms of H_2 evolution. The results indicate that the buffer dependency of electrocatalytic H_2 evolution provides a tool for investigating catalytic pathways in water and also illustrates the importance of buffer choice in optimizing H_2-evolution catalysis.

Results

Cyclic voltammetry of CoMC6*a in water in the presence of varied buffers. Cyclic voltammograms (CVs) of CoMC6*a were collected in water or buffered water with added KCl electrolyte at pH 6.5, a pH at which folding of this mimochrome is optimized.[2,35,36] As previously reported, an irreversible wave results at potentials below –1 V vs. Ag/AgCl (1 M KCl; all potentials will be reported as vs. Ag/AgCl (1 M KCl) unless stated otherwise), corresponding to H_2 evolution catalyzed by CoMC6*a.[2] Here, we note that the half-wave potential (E_h) for the catalytic wave varies significantly in the presence of different buffering agents, over a range of 0.57 V. For clarity, representative data for CoMC6*a in the presence of five selected buffers (50 mM) and without buffer are shown in Figure 2. Results for all 12 buffering agents used herein with pK_a values ranging from 5.8 to 11.6 (**1**-**12**, structures shown in Figure 3) are shown in Figures S1-S12.

The CV of CoMC6*a in the presence of only water and KCl (Figure 2 and Figure S13), yields a wave at E_h = –1.82 V, which is significantly lower than waves observed in the presence of buffer acids **1-12** (Figures S1-12). Table S1 lists the buffer acids **1**-**12** and their corresponding abbreviations, pK_a values, and E_h values obtained from CV data of CoMC6*a at pH 6.5. CV experiments were also performed at pH 5.0, a pH value below the pK_a of the most acidic buffer acid used here, to achieve conditions where each buffer is ≥86% in the conjugate acid form (Figures S14-S26). Table S2 summarizes the E_h values from CV data of CoMC6*a in the presence of **1**-**12** at a constant pH of 5.0, however, the E_h values are within 0.04 V of those measured at pH 6.5.

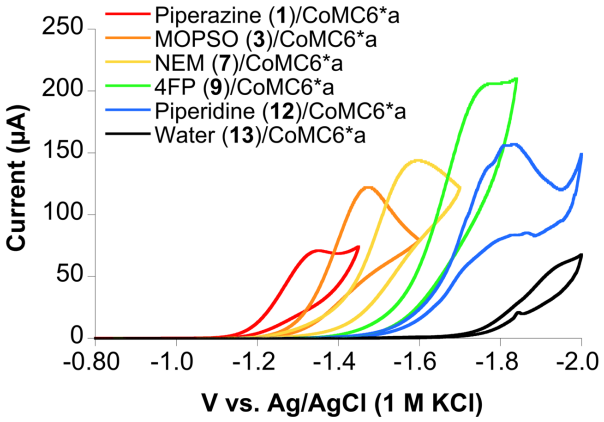

Figure 2. Overlay of CVs of CoMC6*a in the presence of selected buffering agents. The CV data were collected under nitrogen at a 100 mV/s scan rate with 1.0 μM CoMC6*a, 50 mM buffer (when present), 100 mM KCl, pH 6.5. A glassy carbon counter electrode, Ag/AgCl (1 M KCl) reference electrode, and HMDE working electrode were used. Third scan data are shown. For plot of peak currents as a function of pK_a at a constant concentration of the conjugate acid form of the buffers **1**-**12**, see Figs. S45-S46.

Figure 3 shows a plot of the E_h values (Table S1) as a function of buffer acid pK_a at pH 6.5. A potential-pK_a relationship results that can be divided into two regions. For buffer acids of p$K_a \leq$ 8.7, E_h changes as a function of pK_a with a slope of –128 mV/pK_a unit (region 1), and for buffer acids of p$K_a \geq$ 8.7, E_h changes as a function of pK_a with a slope of –39 mV/pK_a unit (region 2). The results obtained at pH 6.5 do not deviate significantly from those at pH 5.0, which is a pH value that is below the pK_a value of the most acidic buffer acid. At pH 5.0, region 1 exhibits a slope of

–123 mV/pK_a unit, and region 2 exhibits a slope of –41 mV/pK_a unit (Figure S27). Equations 1 and 2 outline relationships for a redox-coupled proton transfer process involving complex C, n electrons, and m protons, where the proton is donated to C from an acid HA.[37,38] Equation 2 predicts that the E_h depends on the acid pK_a if the first three terms are constant, where the first term describes the reduction potential of the species C in the absence of protons, the second term describes the pK_a of the protonated and reduced C product, and the third term describes the logarithm of concentration of the base (A^-) over the concentration of the conjugate acid (HA).[38] Comparison of the slopes from data obtained at pH 6.5 and at pH 5.0 indicate that the log(A^-/HA) term must be constant, which is expected under conditions where [HA]>>[A^-], or the concentration of the conjugate acid is much greater than the concentration of the complex of interest, C.[38] Thus, the plot of E_h as a function of the pK_a of the added acid HA is expected to yield a pK_a-dependent region with a slope of 0.059(m/n) at 25 °C (Equation 2). As shown in Figure 3, the slope in region 1 is consistent with a $2H^+/1e^-$ process (theoretical value of –118 mV/pK_a unit), and the magnitude of the slope in region 2 is consistent with a $1H^+/1e^-$ process (theoretical value of –59 mV/pK_a unit).

$$C + mHA + ne^- \rightleftharpoons CH_m^{-(n-m)} + mA \quad (1)$$

$$E_h = E^{\circ\prime}(C^{0/-n}) + 0.059(m/n)[pK_a(CH_m^{-(n-m)}) - \log(A^-/HA) - pK_a(HA)] \quad (2)$$

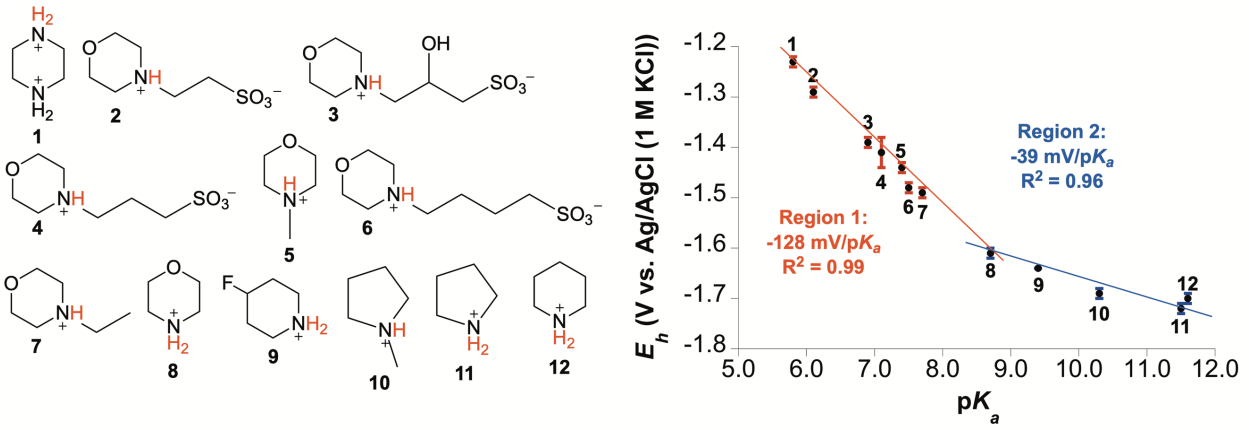

Figure 3. Buffer dependence of catalytic half-wave potential. On the right is a plot of E_h values measured by CV for H_2 evolution at pH 6.5 by CoMC6*a as a function of buffer acid pK_a. Region 1 (solid red line) has a slope of –128 mV/pK_a unit, and region 2 (solid blue line) has a slope of –39 mV/pK_a unit. The red line (region 1) was fitted using E_h values from buffer acids **1**-**8**, and the blue line (region 2) was fitted using E_h values from buffer acids **8**-**12** (structures on the left). The CV data were collected under nitrogen at 100 mV/s scan rate with 1.0 μM CoMC6*a, 50 mM of the buffer, 100 mM KCl, and a pH of 6.5. A glassy carbon counter electrode, Ag/AgCl (1 M KCl) reference electrode, and HMDE working electrode were used. The E_h values are an average of three separate trials with standard deviation bars shown in the plot. The potential-pK_a plots at pH 5.0 are shown in the Figure S27, and the slopes do not deviate significantly from those at pH 6.5.

At pH 6.5, buffers **1**-**4** are 17-80% in the conjugate acid form. Cyclic voltammetry experiments of CoMC6*a were also performed in the presence of **1**-**4** at pH values at least one unit below the pK_a values of buffer acids **1**-**4** (Figures S28-S31). No significant differences were observed between the E_h values at a pH of 6.5 compared to the E_h values from the CVs performed at a pH that is one unit below the pK_a values of **1**-**4**. The potential-pK_a relationship observed in region 1 for a $2H^+/1e^-$ reduction at pH 6.5 (Figure 3) does not change significantly when the data

are plotted using E_h values from these CV data (–105 mV/pK_a unit for region 1, Figure S32). Buffer acid titrations of **1**-**12** were also performed for CV experiments of CoMC6*a at pH 6.5, and the peak current (i_p) increases as a function of increasing buffer acid concentration but no significant shifts in the E_h value as a function of concentration is seen (Figures S33-S44). The conditions used for the titration experiments yield ~1-50 mM of the conjugate acid species at pH 6.5.

The peak currents in the CVs of CoMC6*a in the presence of 50 mM buffer **1**-**12** at pH 5.0 are comparable to each other with no apparent trends as a function of pK_a (Figure S45). In addition, the peak currents as a function of pK_a at a constant pH of 6.5 and constant concentration of the conjugate acid species (50 mM) are also comparable across buffer acids **1**-**12** (Figure S46). The data indicate that the magnitude of the peak current is primarily affected by the availability of the conjugate acid form of the buffers **1**-**12,** regardless of pK_a. The data also indicate that the position of the catalytic half-wave is maintained for a particular buffer acid, despite the changes in the availability of the conjugate acid form of the buffer as a function of buffer concentration at constant pH *or* as a function of changing pH, indicating that the catalytic half-wave potential is primarily dependent on buffer acid pK_a.

Investigation of buffer structure effects. Several amines with structures related to standard buffers were synthesized in order to explore the influence of steric bulk around the acidic proton on catalysis (Scheme 1). The pK_a values of the sterically hindered buffer acids were expected to be similar to those of the parent buffer acids (confirmed by potentiometric titrations, Figures S47-S50), allowing for systematic evaluation of steric bulk on activity. The derivatives are *N-N-tert*-butyl-piperazine (DTBP, **1a**), *N-iso*-propyl-morpholine (IPM, **8a**), *N-tert*-butyl-morpholine (TBM, **8b**), and *N-tert*-butyl-piperidine (TBP, **12a**) (Synthetic details are in the **Materials and Methods** section). To synthesize this series of amines, we devised a new method using a unified approach with relatively high yields compared to those in the literature.[39–43] We describe a succinct method in the **Materials and Methods** section, summarized in Schemes S1 and S2. Characterization through ^{1}H-NMR, ^{13}C-NMR, and potentiometric titration is included in the SI (Figures S47-S60). Potentiometric titrations were also performed for NMM (**4**) and MES (**2**), and the estimated pK_a values were compared to literature values to confirm the accuracy of the potentiometric titration method (Figures S51-S52).

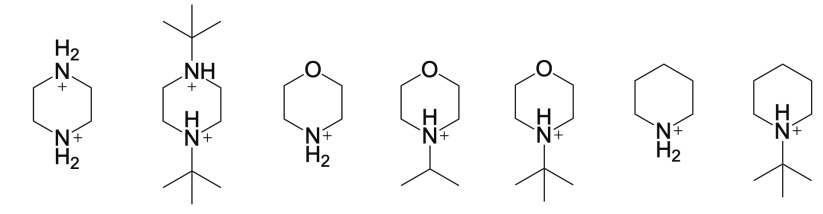

Scheme 1

Table S3 summarizes the pK_a values of **1a**, **8a**, **8b**, and **12a**, and the average E_h and i_p values from CV of CoMC6*a in **1a**, **8a**, **8b**, and **12a** compared to CV in the presence of the respective parent buffer acids **1**, **8**, and **12** (Table S3). Cyclic voltammetry of CoMC6*a in DTBP (**1a**) shows diminished current compared to CoMC6*a in piperazine (**1**), evaluated through the peak current

(Figure 4a). Compared to results obtained in the presence of morpholine (**8**), IPM (**8a**) and TBM (**8b**) also have significantly diminished peak current for the catalytic waves (Figure 4b). Compared to piperidine (**12**), TBP (**12a**) shows diminished current at the same potential for the catalytic wave for CoMC6*a in piperidine, in addition to a catalytic wave that is apparently cathodically shifted relative to CV in the presence of piperidine (Figure 4c). However, at these low potentials, it is possible that this feature corresponds to the catalytic wave for CoMC6*a in only water and KCl electrolyte (Figure S13), as the faradaic current in water and electrolyte begins at an onset of ~–1.70 V. Regardless, the average E_h value is estimated to be –1.80 V. These results indicate that the increased steric bulk at the proton donation site significantly lowers the peak current, which possibly reflects a lower rate of catalysis by CoMC6*a. As the pK_a values of the sterically hindered proton donors are similar to those of the parent proton donors, the effect of increasing bulk near the acidic proton on catalytic current relates to buffer acid structure rather than pK_a. Furthermore, the potential-pK_a relationships noted above are maintained when the E_h values obtained from CV of CoMC6*a in the presence of the sterically hindered buffer acid derivatives are included in the potential-pK_a plot (–114 mV/pK_a unit for region 1 and –33 mV/pK_a unit for region 2, Figure S61). CVs of **1a**, **8a**, **8b**, and **12a** without CoMC6*a are shown in the SI (Figures S62-S64).

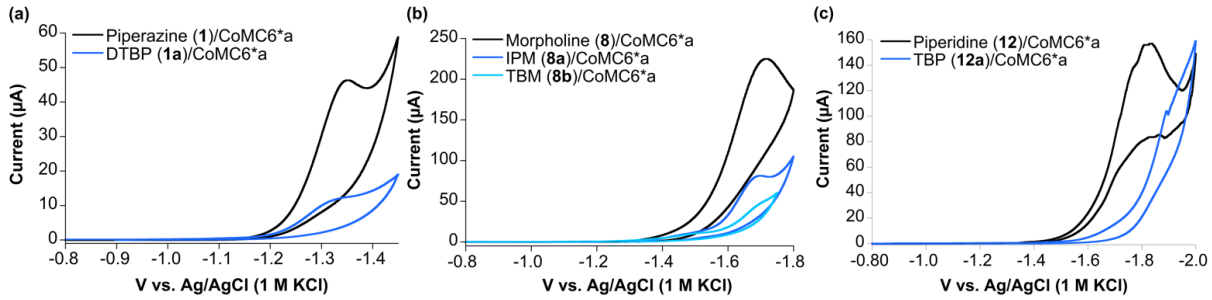

Figure 4. Overlay of CVs of CoMC6*a in the presence of sterically hindered buffer acid compared to the parent buffer acid. The CV data were collected under nitrogen at 100 mV/s scan rate with 1.0 μM CoMC6*a, 50 mM buffer, 100 mM KCl, and a pH of 6.5. A glassy carbon counter electrode, Ag/AgCl (1 M KCl) reference electrode, and HMDE working electrode were used.

Discussion

The most commonly invoked pathways for cobalt-catalyzed electrocatalytic H_2 evolution are denoted the ECCE or ECEC,[21,27,44] where E is an electrochemical step, and C is a chemical step (Scheme 2). A third pathway, EECC, is also possible involving the protonation of a formally Co(0) species, although such a pathway is unlikely in water as the EECC mechanism is typically invoked in systems where the acid is significantly weaker than water.[10,22,45,46] It is challenging to distinguish between the ECCE and ECEC pathways,[47–50] although this has been possible in a few cases where the Co(III)-H reduction to Co(II)-H is cathodic of the Co(II/I) reduction.[51,52]

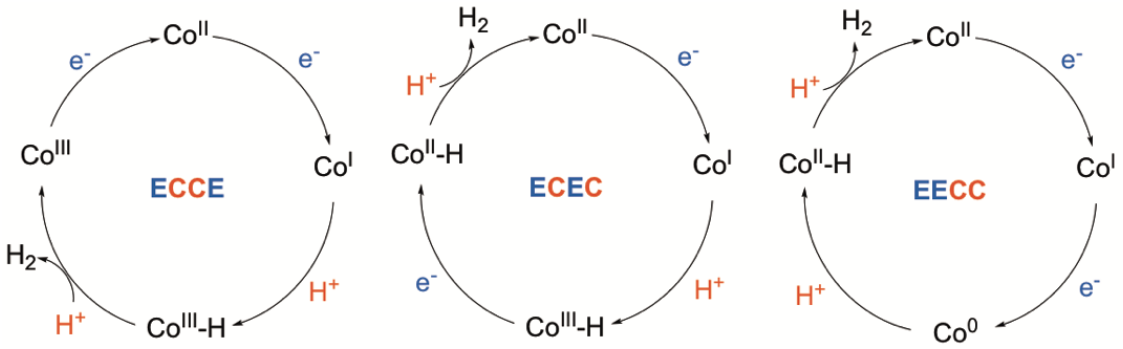

Scheme 2

In a previous report, CV of CoMC6*a in DMF revealed quasi-reversible Co(III/II) and Co(II/I) couples and the assignment of the Co(I) species as the catalytically active species.[2] Although working in water obscures the Co(II/I) couple due to the presence of protons as a substrate, it is likely that Co(I) is the catalytically active species in water, consistent with the appearance of a catalytic wave at low potentials. It is tempting to relate the cobalt-centered mechanisms (Scheme 2) to the reduction events extrapolated from the observed potential-pK_a relationships (Figure 2), but the potential-pK_a relationships can only provide a qualitative evaluation of mechanism, especially when the analyses of electrochemical responses of systems working in water are less straightforward than those that operate in aprotic solvent where electrochemical responses can be directly attributed to a single acid source. Adding to these challenges, multiple mechanisms can coexist.[21,47] However, these relationships can give insight to the predominant mechanisms under certain conditions.

The observed change in slope from –128 mV/pK_a unit (region 1) to –39 mV/pK_a (region 2) we propose to reflect a change from a $2H^+/1e^-$event to a $1H^+/1e^-$event (Figure 3) as pK_a of the buffer acid increases. The difference in slope suggests different mechanisms, and the ECCE and the ECEC mechanisms (Scheme 2) may be considered for region 1 and region 2, respectively, if these potential-pK_a relationships are assumed to be related to metal-centered steps. An additional supposition is that the protonation events in the $2H^+/1e^-$ and $1H^+/1e^-$ cases are related to the Co(II/I) reduction that initiates catalysis. If the observed reduction events are indeed related to the steps that are strictly cobalt-centered, the effects of the proton donor pK_a on mechanism correlate well with the trends observed in other systems, where strong acids can protonate both the Co(I) and Co(III)-H species,[23,24] but use of weak acids requires that the Co(II)-H intermediate must be accessed for H_2 evolution.[24–26] In that case, the stronger buffer acids (p$K_a \leq 8.7$) can protonate the Co(I) and Co(III)-H intermediates to yield H_2 via the ECCE mechanism. The buffer acids that are weaker acids (p$K_a \geq 8.7$) can protonate Co(I) to yield Co(III)-H, but further reduction of the Co(III)-H to the more nucleophilic Co(II)-H species is required to yield H_2. Published work in aprotic solvent provides a useful comparison. In the case of a cobaloxime catalyst, $[Co(dmgBF_2)_2L]$, CV experiments revealed that H_2 is evolved via the ECCE pathway with trifluoroacetic acid as a proton source (pK_a = 12.7 in acetonitrile).[53] A later study revealed that $[Co(dmgBF_2)_2L]$ also evolves H_2 via the ECEC pathway in addition to ECCE.[24] In the same study, $[Co(dmgBF_2)_2L]$ is reported to produce H_2 via ECCE as the predominant pathway using the stronger acid, *p*-cyanoanilinium tetrafluoroborate (pK_a = 7.6 in acetonitrile).[24] These studies

demonstrate that it is plausible that a change in the predominant mechanism can occur for CoMC6*a as a function of buffer acid pK_a value.

In the aforementioned [Co(dmgBF$_2$)$_2$L] system in acetonitrile, the proposed Co(III) + H$_2$/Co(III)-H pK_a of 10.5 is slightly lower than the Co(III)-H/Co(I) pK_a of 13.3, and the Co(II) + H$_2$/Co(II)-H pK_a is 36.3.[24] If the pK_a of the added acid is greater than that of Co(III) + H$_2$/Co(III)-H but less than that of Co(III)-H/Co(I), the acid can protonate Co(I) in the first chemical step but not Co(III)-H in the second chemical step. Thus, Co(II)-H must be accessed for the second protonation by the acid to generate H$_2$. A similar scenario may be invoked for CoMC6*a, where the Co(III) + H$_2$/Co(III)-H pK_a is proposed to be lower than the pK_a of Co(III)-H/Co(I). If the observed change in slope of the E_h vs. pK_a plot indicates a change in mechanism from ECCE to ECEC, then the Co(III) + H$_2$/Co(III)-H pK_a can be estimated from the point at which the two slopes intersect (Figure 3), which is ~8.7. Specifically, buffer acids with p$K_a \leq 8.7$ can protonate both Co(I) and Co(III)-H in the ECC steps in the ECCE pathway, and proton donors with pK_a values beyond 8.7 can only protonate Co(I) in the first EC step of ECEC, and Co(II)-H must be accessed to yield H$_2$ in this case.

For the more basic buffer acids (p$K_a \geq 8.7$), the slope of the E_h vs. pK_a plot is indicative of a 1H$^+$/1e$^-$ reduction and is seen for all of the buffers tested here (up to a pK_a of 11.6 and E_h of –1.73 V). If the 1H$^+$/1e$^-$ reduction is related to the Co(II/I) reduction, the continued change in E_h as a function of pK_a beyond 8.7 implies that the Co(III)-H/Co(I) pK_a is greater than that of Co(III) + H$_2$/Co(III)-H. In theory, the pK_a of Co(III)-H/Co(I) species could be found by testing buffer acids with greater pK_a values, but the leveling effect of water as a solvent sets a maximum pK_a at 14.0.[54] In addition, the fact that an onset potential of –1.70 V and a half-wave potential of –1.82 V at pH 6.5 are observed in the CV of CoMC6*a in water and electrolyte (no buffer) makes analysis of catalytic peaks difficult if there are catalytic waves much beyond –1.70 V. However, we speculate that it is possible that the Co(II/I) reduction potential can be more cathodic than –1.73 V based on the end point of pK_a 11.6 in region 2. Activity is observed for CoMC6*a even in water and no buffer acid with a E_h value of –1.82 V (Figure 2). A potential of –1.82 V is surprisingly low, but the Co(II/I) potential of CoMC6*a was observed to be –2.64 V vs. Fc/Fc$^+$ in DMF,[2] which is significantly more negative than the Co(II/I) potential for the [Co(dmgBF$_2$)$_2$L] catalyst (~–2 V vs. Fc/Fc$^+$ in DMF).[24]

One case implicating a pK_a for Co(III)-H/Co(I) in water involves a cobalt bis(iminopyridine) complex.[55] At pH values ≥ 7, the primary route for H$_2$ generation begins with protonation by H$_3$O$^+$ when the Co(I) species is further reduced at the ligand to yield a Co-H species that the authors describe as [Co(III)-H(L$_4^{\bullet-}$)]$^{1+}$. Below pH 6, direct protonation of Co(I) occurs to generate [Co(III)-H(L$_4$)]$^{2+}$, implying that the Co(III)-H/Co(I) pK_a may be between 6 and 7. Although it is not evident mechanistically from this work how H$_2$ is evolved after the first protonation event occurs, it sheds light on the pK_a of Co(III)-H/Co(I) for a cobalt catalyst working in water. This pK_a for the cobalt bis(iminopyridine) complex is lower than what is implicated for the Co(III)-H/Co(I) pK_a for CoMC6*a, but the Co(II/I) reduction potential for the cobalt bis(iminopyridine) complex is observed at –1.05 V vs. SCE (~–1.0 V vs. Ag/AgCl (1 M KCl)) at pH 7.0 (overpotential of 0.39 V). For CoMC6*a, the Co(II/I) potential may be as low as –1.82 V vs. Ag/AgCl (1 M KCl) at pH 6.5 (overpotential of 1.2 V). It has been reported that the Co(II/I) reduction potential is directly correlated with the pK_a for Co(III)-H/Co(I), where lower potentials correspond to higher pK_a values.[56] Thus, it is plausible that the Co(III)-H/Co(I) pK_a for CoMC6*a is greater than that of the cobalt bis(iminopyridine) complex.

In the presence of the buffer acids, **1a**, **8a**, **8b**, and **11a** with steric bulk at the acidic proton of the amine, CoMC6*a displayed lower activity as reflected by peak current in CV when compared to CV in the presence of the parent buffer acids. The lower peak current in the presence of sterically hindered buffer acids provides further evidence that the buffer acid acts as a proton donor to CoMC6*a. As demonstrated most clearly for derivatives of piperazine and morpholine, the peak current of the catalytic waves is diminished in the sterically hindered derivatives (Figures 4a-4b), but the position of the catalytic half-wave is broadly maintained with respect to the pK_a (Figure S61). These results indicate that the driving force for catalysis is dependent on the pK_a of the proton donor, and that the structure of the proton donor may impact the rate.

The invariant nature of the E_h as a function of the buffer acid concentration for a given buffer acid (Figures S33-S44) in conjunction with the fact that the peak currents show no trend across proton donors **1**-**12** when the concentration of the conjugate acid form of the proton donors is held constant, indicates that the protonation steps may not be rate-limiting despite the strong evidence that the rate-limiting steps in H_2-evolution catalysis often involve the protonation steps.[46,57] This surprising outcome may be attributed to the CoMC6*a peptide scaffold having a role in catalysis by possibly positioning the proton donors for favorable interaction with the active site such that proton transfer would not be rate-limiting. A conformational change of CoMC6*a may be necessary for this to occur. The effect of the sterically hindered proton donors on lowering the peak current as a function of steric bulk at the proton donation site supports the idea that the peptide scaffold has a role in positioning the buffer acid for proton transfer. As shown previously, it is clear that the peptide scaffold plays a role in catalysis, evidenced by the effect of CoMC6*a folding on catalytic potential.[2]

Conclusions

We have shown that the potential required for H_2 evolution by the synthetic mini-enzyme CoMC6*a is dramatically changed by the addition of an exogenous proton donor in water. Furthermore, the dependence of the catalytic half-wave potential on proton donor pK_a falls into two different regimes consistent with different H_2-evolution pathways. In addition, the steric bulk of the proton donor has an impact on the catalytic current. These results indicate that the pK_a and structure of the buffer used should be considered when developing and evaluating systems in water for proton-requiring catalysis. As demonstrated by a water-stable iron tetraphenylporphyrin system for CO_2 reduction, buffer choice can even tune selectivity between CO or H_2 formation.[58] In the case evaluated herein, the buffer can also provide a handle into probing HER mechanism, as demonstrated by the strong dependence of the catalytic half-wave potential on proton donor pK_a and the differing potential-pK_a relationships that arise.

Materials and Methods

Synthesis and characterization CoMC6*a. Synthesis and characterization of CoMC6*a are previously described.[2,35]

Cyclic voltammetry. Cyclic voltammetry experiments in water were performed with a hanging mercury drop working electrode (HMDE) from BASi Instruments. The counter electrode used was a 3 mm glassy carbon electrode from CH Instruments, Inc. The counter electrode was polished with 0.05 micron Gamma alumina paste before each experiment. The reference electrode used is

a Ag/AgCl (1 M KCl) from CH Instruments, Inc. The general procedure for CV is as follows: 5.0 mL of 1.0 μM CoMC6*a in 100 mM KCl and 50 mM buffer at pH 6.5 was used unless stated otherwise. The CV scan rate was 100 mV/s. Each measurement used a fresh mercury drop with an average mass of 5.6 $\pm$ 1.3 mg. Before each experiment, the solution was purged for 5 minutes with nitrogen, and the measurements were performed under a blanket of nitrogen. The pH was monitored using a VWR SB70P pH meter and a Mettler Toledo InLab semimicro pH probe. All E_h and i_p values from CV data with CoMC6*a were determined after subtraction of the CV without CoMC6*a.

Synthesis of *N*-substituted morpholine and piperidine. A sealed pressure tube was charged with a stirring bar, dihaloalkane **S** (1 equiv.) and primary amine (4 equiv.) (Scheme S1). The tube was sealed and heated to 95 °C (R = *t*Bu) or 85 °C (R = *i*Pr) under vigorous stirring behind a blast shield. The reaction was monitored by ^{1}H-NMR until full consumption of dihaloalkane **S** had occurred, upon which the reaction was cooled. Hexanes (roughly equal to five times the initial reaction volume) was added, along with a similar volume of aqueous 1.0 M HCl. The organic layer was separated and then extracted twice more with aqueous 1.0 M HCl, each with the same volume as the initial extraction. The pH of the combined aqueous layer was adjusted with solid NaOH until a pH of roughly 14. The basic aqueous layer was extracted three times with dichloromethane (DCM) and the combined organic layer was dried over $MgSO_4$, filtered over a fritted funnel, and the filtrate was concentrated by rotary evaporation to remove solvent and the volatile excess primary amine. The amine liquor that was obtained was sufficiently pure tertiary amine *N-tert*-butyl-morpholine (TBM, **8b**), *N-tert*-butyl-piperidine (TBP, **12a**) or *N-iso*-propyl-morpholine (IPM, **8a**). The dihaloalkanes **S**, primary amine starting materials, and tertiary amines are not UV active, thus they were visualized by phosphomolybdic acid (PMA) or $KMnO_4$ staining on TLC. All products matched literature ^{1}H-NMR and ^{13}C-NMR data (Figures S53-58).

Synthesis of *N-N-tert*-butyl-piperazine. *N,N-tert*-butylethylenediamine (1 equiv.) and 1,2-dibromoethane (4 equiv.) were combined in a round-bottom flask fitted with a reflux condenser and heated to 100 °C while magnetically stirring for 18 h (Scheme S2). The reaction was monitored by ^{1}H-NMR until full consumption of *N,N-tert*-butylethylenediamine had occurred, upon which the reaction was cooled. Hexanes (roughly equal to five times the initial reaction volume) was added, along with a similar volume of aqueous 1.0 M HCl. The organic layer was separated and then extracted twice more with aqueous 1.0 M HCl, each with the same volume as the initial extraction. The pH of the combined aqueous layer was adjusted with solid NaOH until a pH of roughly 14. The basic aqueous layer was extracted three times with dichloromethane, and the combined organic layer was dried over $MgSO_4$, filtered over a fritted funnel, and concentrated by rotary evaporation to remove solvent. The resulting waxy residue was loaded onto a fritted funnel containing a pad of SiO_2 (15 x crude material mass by dry weight, packed as a gel with EtOAc), and a dry column vacuum chromatography separation was conducted in 50 mL EtOAc fractions. The first four fractions contained pure product by TLC visualized with $KMnO_4$ stain. These fractions were combined and concentrated by rotary evaporation to yield *N,N-tert*-butyl-piperazine (DTBP, **1a**) as a powdery white solid (49% yield). The dibromoethane, amine starting material, and tertiary diamine product are not UV active, thus they were visualized by PMA or $KMnO_4$ staining on TLC. The product matched literature ^{1}H-NMR and ^{13}C-NMR data (Figures S59-S60).

pK_a estimation of TBM, IPM, TBP, and DTBP. The pK_a values of buffer acids TBM (**8b**), IPM (**8a**), TBP (**12a**), and DTBP (**1a**) were estimated by potentiometric titration using HCl titrated into the buffer (concentrations and volumes for each material are mentioned in Figures S47-S50). In order to assess the accuracy of this method, the pK_a values of NMM (**5**) and MES (**2**) were also determined and compared to literature values (Figures S51-52). The pH was monitored using a VWR SB70P pH meter and a Mettler Toledo InLab semimicro pH probe. The equivalence points were determined by plotting the pH as a function of volume of acid or base added and taking the first derivative of the plot.

Acknowledgments

We would like to thank Jose L. Alvarez-Hernandez for helpful discussions. This work is supported by the Chemical Sciences, Geosciences and Biosciences Division, Office of Basic Energy Sciences, Office of Science, U.S. Department of Energy, Grant No. DE-FG02-09ER16121.

References

(1) Kandemir, B., Kubie, L., Guo, Y., Sheldon, B., and Bren, K. L. (2016) Hydrogen Evolution from Water under Aerobic Conditions Catalyzed by a Cobalt ATCUN Metallopeptide. *Inorg. Chem. 55*, 1355–1357.
(2) Firpo, V., Le, J. M., Pavone, V., Lombardi, A., and Bren, K. L. (2018) Hydrogen evolution from water catalyzed by cobalt-mimochrome VI*a, a synthetic mini-protein. *Chem. Sci. 9*, 8582–8589.
(3) Boralugodage, N. P., Arachchige, R. J., Dutta, A., Buchko, G. W., and Shaw, W. J. (2017) Evaluating the role of acidic, basic, and polar amino acids and dipeptides on a molecular electrocatalyst for H_2 oxidation. *Catal. Sci. Technol. 7*, 1108–1121.
(4) Ahmed, M. E., Dey, S., Darensbourg, M. Y., and Dey, A. (2018) Oxygen-Tolerant H_2 Production by [FeFe]-H_2ase Active Site Mimics Aided by Second Sphere Proton Shuttle. *J. Am. Chem. Soc. 140*, 12457–12468.
(5) Lakadamyali, F., Kato, M., Muresan, N. M., and Reisner, E. (2012) Selective Reduction of Aqueous Protons to Hydrogen with a Synthetic Cobaloxime Catalyst in the Presence of Atmospheric Oxygen. *Angew. Chemie Int. Ed. 51*, 9381–9384.
(6) McNamara, W. R., Han, Z., Alperin, P. J., Brennessel, W. W., Holland, P. L., and Eisenberg, R. (2011) A Cobalt Dithiolene Complex for the Photocatalytic and. *J. Am. Chem. Soc. 133*, 15368–15371.
(7) Ahmed, M. E., Chattopadhyay, S., Wang, L., Brazzolotto, D., Pramanik, D., Aldakov, D., Fize, J., Morozan, A., Gennari, M., Duboc, C., Dey, A., and Artero, V. (2018) Hydrogen Evolution from Aqueous Solutions Mediated by a Heterogenized [NiFe]-Hydrogenase Model: Low pH Enables Catalysis through an Enzyme-Relevant Mechanism. *Angew. Chemie Int. Ed. 57*, 16001–16004.
(8) Solis, B. H., Maher, A. G., Honda, T., Powers, D. C., Nocera, D. G., and Hammes-Schiffer, S. (2014) Theoretical Analysis of Cobalt Hangman Porphyrins: Ligand Dearomatization and Mechanistic Implications for Hydrogen Evolution. *ACS Catal. 4*, 4516–4526.
(9) Solis, B. H., Maher, A. G., Dogutan, D. K., Nocera, D. G., and Hammes-Schiffer, S. (2016) Nickel phlorin intermediate formed by proton-coupled electron transfer in hydrogen evolution mechanism. *Proc. Natl. Acad. Sci. 113*, 485–492.
(10) Bediako, D. K., Solis, B. H., Dogutan, D. K., Roubelakis, M. M., Maher, A. G., Lee, C. H., Chambers, M. B., Hammes-Schiffer, S., and Nocera, D. G. (2014) Role of pendant proton relays and proton-coupled electron transfer on the hydrogen evolution reaction by nickel hangman porphyrins. *Proc. Natl. Acad. Sci. 111*, 15001–15006.
(11) Helm, M. L., Stewart, M. P., Bullock, R. M., DuBois, M. R., and DuBois, D. L. (2011) A Synthetic Nickel Electrocatalyst with a Turnover Frequency Above 100,000 s^{-1} for H_2 Production. *Science (80-.). 333*, 863–866.
(12) Jackson, M. N., Jung, O., Lamotte, H. C., and Surendranath, Y. (2019) Donor-Dependent Promotion of Interfacial Proton-Coupled Electron Transfer in Aqueous Electrocatalysis. *ACS Catal. 9*, 3737–3743.
(13) Wang, D., and Groves, J. T. (2013) Efficient water oxidation catalyzed by homogeneous cationic cobalt porphyrins with critical roles for the buffer base. *Proc. Natl. Acad. Sci. 110*, 15579–15584.
(14) Chen, Z., Concepcion, J. J., Hu, X., Yang, W., Hoertz, P. G., and Meyer, T. J. (2010) Concerted O atom-proton transfer in the O--O bond forming step in water oxidation. *Proc. Natl.*

Acad. Sci. 107, 7225–7229.
(15) Song, N., Concepcion, J. J., Binstead, R. A., Rudd, J. A., Vannucci, A. K., Dares, C. J., Coggins, M. K., and Meyer, T. J. (2015) Base-enhanced catalytic water oxidation by a carboxylate–bipyridine Ru(II) complex. *Proc. Natl. Acad. Sci. 112*, 4935–4940.
(16) Wang, J.-W., Zhang, X.-Q., Huang, H.-H., and Lu, T.-B. (2016) A Nickel(II) Complex as a Homogeneous Electrocatalyst for Water Oxidation at Neutral pH: Dual Role of HPO_4^{2-} in Catalysis. *ChemCatChem 8*, 3287–3293.
(17) Zhang, L.-H., Yu, F., Shi, Y., Li, F., and Li, H. (2019) Base-enhanced electrochemical water oxidation by a nickel complex in neutral aqueous solution. *Chem. Commun. 55*, 6122–6125.
(18) Schneider, C. R., Lewis, L. C., and Shafaat, H. S. (2019) The good, the neutral, and the positive: buffer identity impacts CO_2 reduction activity by nickel(II) cyclam. *Dalt. Trans.*
(19) Jonsson, B.-H., Steiner, H., and Lindskog, S. (1976) Participation of buffer in the catalytic mechanism of carbonic anhydrase. *FEBS Lett. 64*, 310–314.
(20) Porras, S. P., and Kenndler, E. (2005) Capillary electrophoresis in N,N-dimethylformamide. *Electrophoresis 26*, 3279–3291.
(21) Queyriaux, N., Jane, R. T., Massin, J., Artero, V., and Chavarot-Kerlidou, M. (2015) Recent developments in hydrogen evolving molecular cobalt(II)–polypyridyl catalysts. *Coord. Chem. Rev. 304–305*, 3–19.
(22) Artero, V., Chavarot-Kerlidou, M., and Fontecave, M. (2011) Splitting Water with Cobalt. *Angew. Chemie Int. Ed. 50*, 7238–7266.
(23) Dempsey, J. L., Brunschwig, B. S., Winkler, J. R., and Gray, H. B. (2009) Hydrogen Evolution Catalyzed by Cobaloximes. *Acc. Chem. Res. 42*, 1995–2004.
(24) Baffert, C., Artero, V., and Fontecave, M. (2007) Cobaloximes as Functional Models for Hydrogenases. 2. Proton Electroreduction Catalyzed by Difluoroborylbis(dimethylglyoximato)cobalt(II) Complexes in Organic Media. *Inorg. Chem. 46*, 1817–1824.
(25) Fihri, A., Artero, V., Razavet, M., Baffert, C., Leibl, W., and Fontecave, M. (2008) Cobaloxime-Based Photocatalytic Devices for Hydrogen Production. *Angew. Chemie Int. Ed. 47*, 564–567.
(26) Dempsey, J. L., Winkler, J. R., and Gray, H. B. (2010) Mechanism of H_2 Evolution from a Photogenerated Hydridocobaloxime. *J. Am. Chem. Soc. 132*, 101110100755001.
(27) Costentin, C., Dridi, H., and Savéant, J.-M. (2014) Molecular Catalysis of H_2 Evolution: Diagnosing Heterolytic versus Homolytic Pathways. *J. Am. Chem. Soc. 136*, 13727–13734.
(28) DuBois, D. L. (2014) Development of Molecular Electrocatalysts for Energy Storage. *Inorg. Chem. 53*, 3935–3960.
(29) Bacchi, M., Berggren, G., Niklas, J., Veinberg, E., Mara, M. W., Shelby, M. L., Poluektov, O. G., Chen, L. X., Tiede, D. M., Cavazza, C., Field, M. J., Fontecave, M., and Artero, V. (2014) Cobaloxime-Based Artificial Hydrogenases. *Inorg. Chem. 53*, 8071–8082.
(30) Sommer, D. J., Vaughn, M. D., and Ghirlanda, G. (2014) Protein secondary-shell interactions enhance the photoinduced hydrogen production of cobalt protoporphyrin IX. *Chem. Commun. 50*, 15852–15855.
(31) Kleingardner, J. G., Kandemir, B., and Bren, K. L. (2014) Hydrogen evolution from neutral water under aerobic conditions catalyzed by cobalt microperoxidase-11. *J. Am. Chem. Soc. 136*, 4–7.
(32) Bren, K. L. (2015) Multidisciplinary approaches to solar hydrogen. *Interface Focus 5*, 20140091.

(33) Maeda, K., and Domen, K. (2010) Photocatalytic Water Splitting: Recent Progress and Future Challenges. *J. Phys. Chem. Lett. 1*, 2655–2661.
(34) Le, J. M., and Bren, K. L. (2019) Engineered Enzymes and Bioinspired Catalysts for Energy Conversion. *ACS Energy Lett.* acsenergylett.9b01308.
(35) Caserta, G., Chino, M., Firpo, V., Zambrano, G., Leone, L., D'Alonzo, D., Nastri, F., Maglio, O., Pavone, V., and Lombardi, A. (2018) Enhancement of Peroxidase Activity in Artificial Mimochrome VI Catalysts through Rational Design. *ChemBioChem 19*, 1823–1826.
(36) Leone, L., D'Alonzo, D., Balland, V., Zambrano, G., Chino, M., Nastri, F., Maglio, O., Pavone, V., and Lombardi, A. (2018) Mn-Mimochrome VI*a: An Artificial Metalloenzyme With Peroxygenase Activity. *Front. Chem. 6*.
(37) Weinberg, D. R., Gagliardi, C. J., Hull, J. F., Murphy, C. F., Kent, C. A., Westlake, B. C., Paul, A., Ess, D. H., McCafferty, D. G., and Meyer, T. J. (2012) Proton-Coupled Electron Transfer. *Chem. Rev. 112*, 4016–4093.
(38) McCarthy, B. D., and Dempsey, J. L. (2017) Decoding Proton-Coupled Electron Transfer with Potential–pKa Diagrams. *Inorg. Chem. 56*, 1225–1231.
(39) Suzuki, K., Okano, K., Nakai, K., Terao, Y., and Sekiya, M. (1983) Reductive Rearrangement of 2-Chloroalkanamides with Lithium Aluminum Hydride Leading to α-Methyl-Branched Aliphatic Amines. *Synthesis (Stuttg). 1983*, 723–725.
(40) Denton, S. M. (1999) A Modified Bouveault Reaction for the Preparation of α,α-Dimethylamines from Amides. *Synlett 1999*, 55–56.
(41) Bilke, J. L., and O'Brien, P. (2008) On the Two-Ligand Catalytic Asymmetric Deprotonation of N -Boc Pyrrolidine: Probing the Effect of the Stoichiometric Ligand †. *J. Org. Chem. 73*, 6452–6454.
(42) Carpino, L. A., Ionescu, D., and El-Faham, A. (1996) Peptide Coupling in the Presence of Highly Hindered Tertiary Amines. *J. Org. Chem. 61*, 2460–2465.
(43) Denk, M. K., Krause, M. J., Niyogi, D. F., and Gill, N. K. (2003) Reaction of 1,2-dibromoethane with primary amines: formation of N, N ′-disubstituted ethylenediamines RNH–CH_2CH_2 –NHR and homologous polyamines RNH–[CH_2CH_2NR]n –H. *Tetrahedron 59*, 7565–7570.
(44) Maher, A. G., Passard, G., Dogutan, D. K., Halbach, R. L., Anderson, B. L., Gagliardi, C. J., Taniguchi, M., Lindsey, J. S., and Nocera, D. G. (2017) Hydrogen Evolution Catalysis by a Sparsely Substituted Cobalt Chlorin. *ACS Catal. 7*, 3597–3606.
(45) Lee, C. H., Dogutan, D. K., and Nocera, D. G. (2011) Hydrogen Generation by Hangman Metalloporphyrins. *J. Am. Chem. Soc. 133*, 8775–8777.
(46) Costentin, C., and Savéant, J.-M. (2014) Multielectron, Multistep Molecular Catalysis of Electrochemical Reactions: Benchmarking of Homogeneous Catalysts. *ChemElectroChem 1*, 1226–1236.
(47) Marinescu, S. C., Winkler, J. R., and Gray, H. B. (2012) Molecular mechanisms of cobalt-catalyzed hydrogen evolution. *Proc. Natl. Acad. Sci. 109*, 15127–15131.
(48) King, A. E., Surendranath, Y., Piro, N. A., Bigi, J. P., Long, J. R., and Chang, C. J. (2013) A mechanistic study of proton reduction catalyzed by a pentapyridine cobalt complex: evidence for involvement of an anation-based pathway. *Chem. Sci. 4*, 1578.
(49) Razavet, M., Artero, V., and Fontecave, M. (2005) Proton Electroreduction Catalyzed by Cobaloximes: Functional Models for Hydrogenases. *Inorg. Chem. 44*, 4786–4795.
(50) Muckerman, J. T., and Fujita, E. (2011) Theoretical studies of the mechanism of catalytic hydrogen production by a cobaloxime. *Chem. Commun. 47*, 12456.

(51) Koelle, U., and Paul, S. (1986) Electrochemical reduction of protonated cyclopentadienylcobalt phosphine complexes. *Inorg. Chem. 25*, 2689–2694.
(52) Wiedner, E. S., Appel, A. M., DuBois, D. L., and Bullock, R. M. (2013) Thermochemical and Mechanistic Studies of Electrocatalytic Hydrogen Production by Cobalt Complexes Containing Pendant Amines. *Inorg. Chem. 52*, 14391–14403.
(53) Hu, X., Cossairt, B. M., Brunschwig, B. S., Lewis, N. S., and Peters, J. C. (2005) Electrocatalytic hydrogen evolution by cobalt difluoroboryl-diglyoximate complexes. *Chem. Commun*. 4723.
(54) Moran, M. J. (2006) Factors That Influence Relative Acid Strength in Water: A Simple Model. *J. Chem. Educ. 83*, 800.
(55) Stubbert, B. D., Peters, J. C., and Gray, H. B. (2011) Rapid Water Reduction to H_2 Catalyzed by a Cobalt Bis(iminopyridine) Complex. *J. Am. Chem. Soc. 133*, 18070–18073.
(56) Solis, B. H., and Hammes-Schiffer, S. (2011) Substituent Effects on Cobalt Diglyoxime Catalysts for Hydrogen Evolution. *J. Am. Chem. Soc. 133*, 19036–19039.
(57) Rountree, E. S., McCarthy, B. D., Eisenhart, T. T., and Dempsey, J. L. (2014) Evaluation of Homogeneous Electrocatalysts by Cyclic Voltammetry. *Inorg. Chem. 53*, 9983–10002.
(58) Costentin, C., Robert, M., Savéant, J.-M., and Tatin, A. (2015) Efficient and selective molecular catalyst for the CO_2 -to-CO electrochemical conversion in water. *Proc. Natl. Acad. Sci. 112*, 6882–6886.

Supporting Information for

Buffer Acid Dependence of Hydrogen Evolution from Water Catalyzed by a Cobalt Mini-enzyme

Jennifer M. Le,[a] Georgios Alachouzos,[a] Alison J. Frontier,[a] Angela Lombardi,[b] and Kara L. Bren[a]*

[a]*Department of Chemistry, University of Rochester, Rochester, NY 14627, USA*

[b]*Department of Chemical Sciences, University of Naples Federico II, Complesso Universitario Monte S. Angelo, via Cintia 45, 80126 Naples, Italy*

General Experimental Details

Cyclic voltammetry data were collected under nitrogen at a 100 mV/s scan rate with 1.0 μM CoMC6*a and 100 mM KCl. A glassy carbon counter electrode, Ag/AgCl (1 M KCl) reference electrode, and HMDE working electrode were used. The plots display third scan data. Cyclic voltammetry experiments of buffer acid titrations were also performed with these conditions with varying buffer acid concentrations. All reported E_h values are an average of three separate trials.

CVs of CoMC6*a in the presence of buffer acids 1-12 and water at pH 6.5

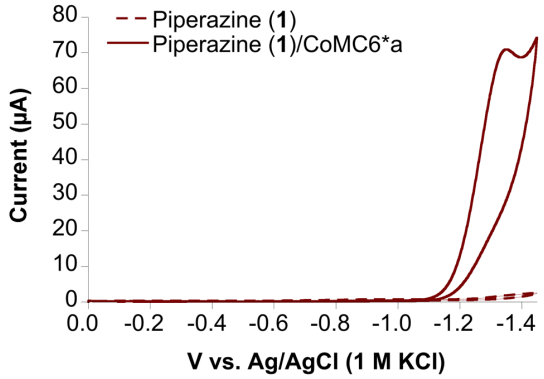

Figure S1. Cyclic voltammogram of CoMC6*a in 50 mM piperazine (**1**) at pH 6.5.

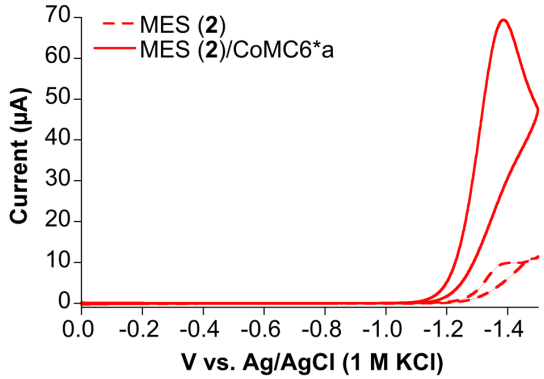

Figure S2. Cyclic voltammogram of CoMC6*a in 50 mM MES (**2**) at pH 6.5.

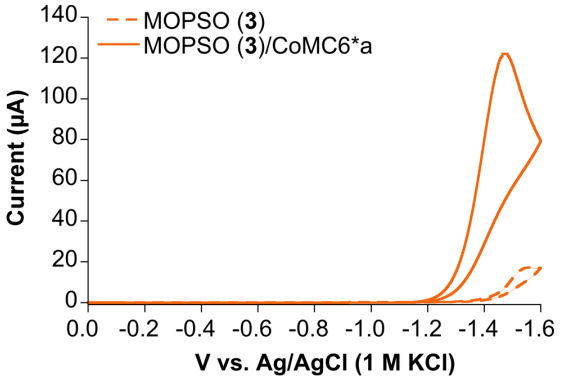

Figure S3. Cyclic voltammogram of CoMC6*a in 50 mM MOPSO (**3**) at pH 6.5.

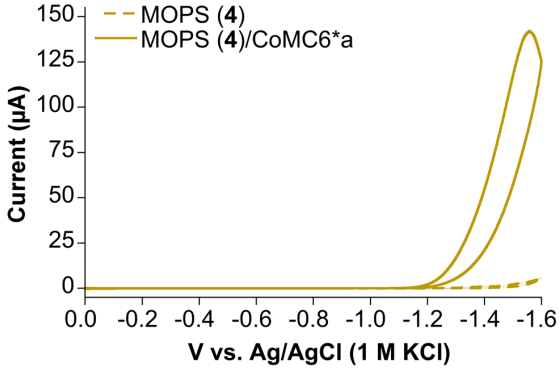

Figure S4. Cyclic voltammogram of CoMC6*a in 50 mM MOPS (**4**) at pH 6.5.

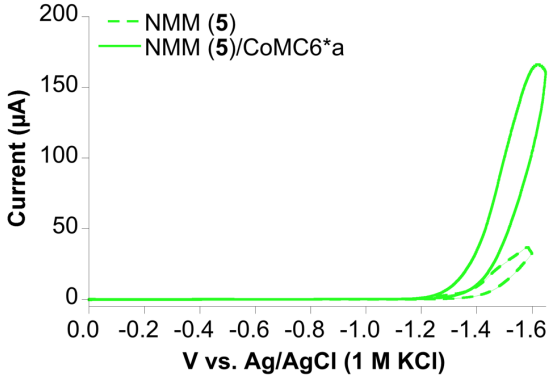

Figure S5. Cyclic voltammogram of CoMC6*a in 50 mM NMM (**5**) at pH 6.5.

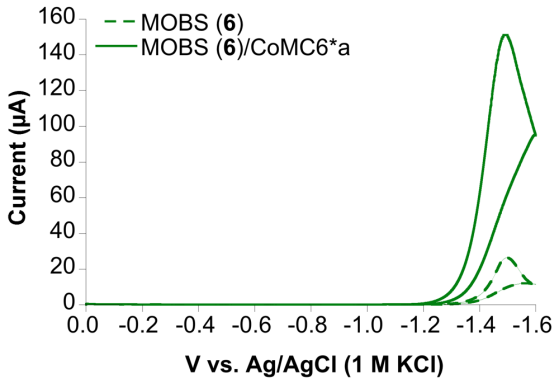

Figure S6. Cyclic voltammogram of CoMC6*a in 50 mM MOBS (**6**) at pH 6.5.

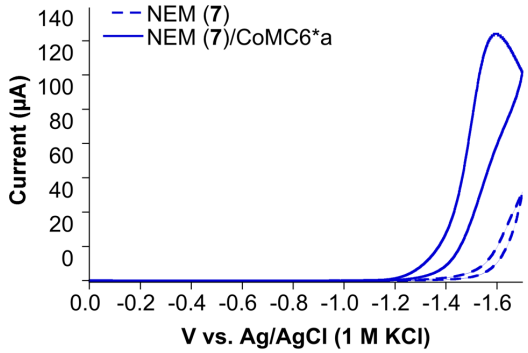

Figure S7. Cyclic voltammogram of CoMC6*a in 50 mM NEM (**7**) at pH 6.5.

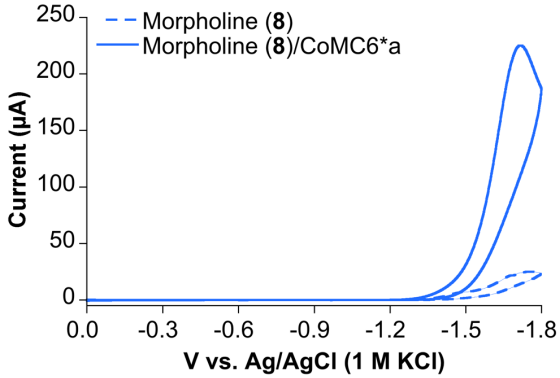

Figure S8. Cyclic voltammogram of CoMC6*a in 50 mM morpholine (**8**) at pH 6.5.

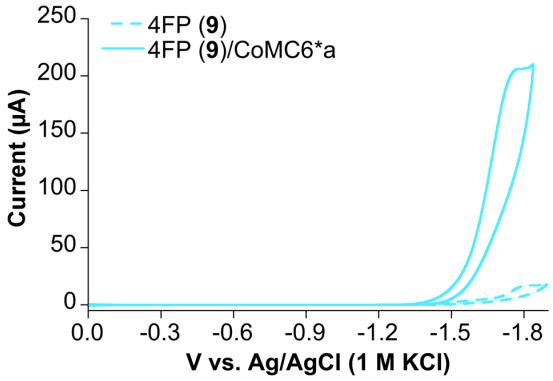

Figure S9. Cyclic voltammogram of CoMC6*a in 50 mM 4FP (**9**) at pH 6.5.

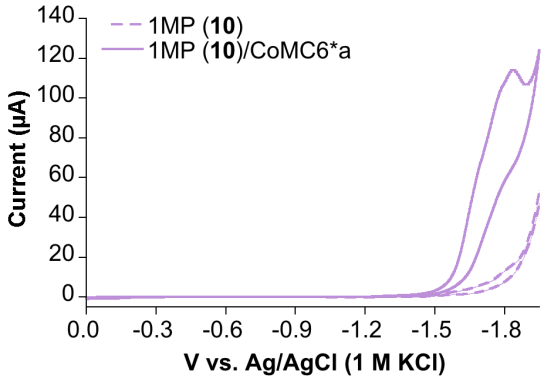

Figure S10. Cyclic voltammogram of CoMC6*a in 50 mM 1MP (**10**) at pH 6.5.

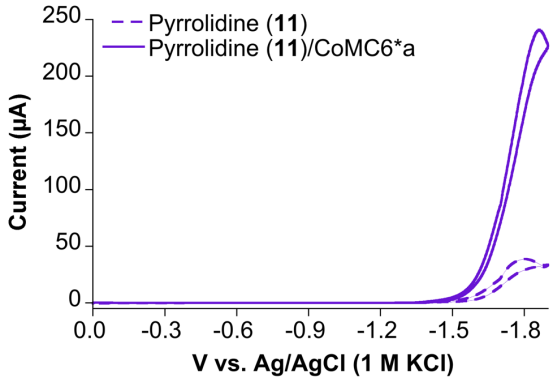

Figure S11. Cyclic voltammogram of CoMC6*a in 50 mM pyrrolidine (**11**) at pH 6.5.

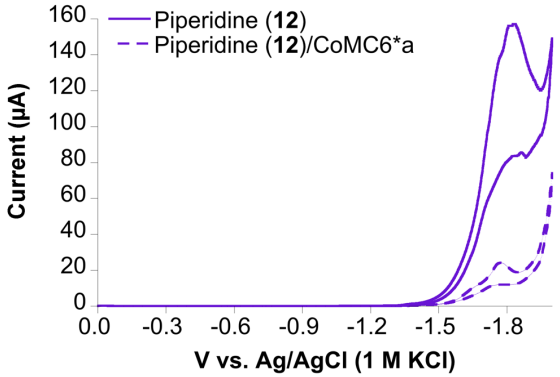

Figure S12. Cyclic voltammogram of CoMC6*a in 50 mM piperidine (**12**) at pH 6.5.

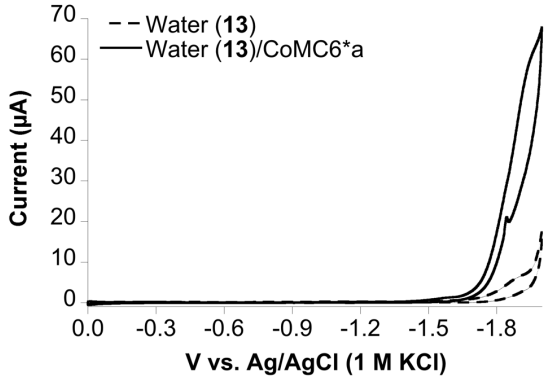

Figure S13. Cyclic voltammogram of CoMC6*a in water (**13**) at pH 6.5.

Table S1. Buffer acids and their corresponding abbreviations used in this work, pK_a, and average E_h values. All E_h data are from CVs that were collected under nitrogen at 100 mV/s scan rate with 1.0 μM CoMC6*a, 50 mM buffer, 100 mM KCl, and a pH of 6.5. A glassy carbon counter electrode, Ag/AgCl (1 M KCl) reference electrode, and HMDE working electrode were used. The E_h values are an average of three separate runs.

Buffer acids	Abbreviation	pK_a	E_h (V vs. Ag/AgCl (1 M KCl)) ± STD DEV
1. Piperazine	–	5.8*	–1.23 ± 0.01
2. 2-(*N*-morpholino)ethanesulfonic acid	MES	6.1	–1.29 ± 0.01
3. 3-morpholino-2-hydroxypropanesulfonic acid	MOPSO	6.9	–1.39 ± 0.01
4. 3-morpholinopropane-1-sulfonic acid	MOPS	7.1	–1.41 ± 0.03
5. *N*-methylmorpholine	NMM	7.4	–1.44 ± 0.01
6. 4-(*N*-morpholino)butanesulfonic acid	MOBS	7.5	–1.48 ± 0.01
7. *N*-ethylmorpholine	NEM	7.7	–1.49 ± 0.01
8. Morpholine	–	8.7	–1.61 ± 0.01
9. 4-fluoropiperidine	4FP	9.4	–1.64 ± 0.00
10. 1-methylpyrrolidine	1MP	10.3	–1.69 ± 0.01
11. Pyrrolidine	–	11.5	–1.71 ± 0.01
12. Piperidine	–	11.6	–1.73 ± 0.01
13. Water	–	14.0	–1.82 ± 0.03

*pK_a 1

CVs of CoMC6*a in buffer acids 1-12 and water at pH 5.0

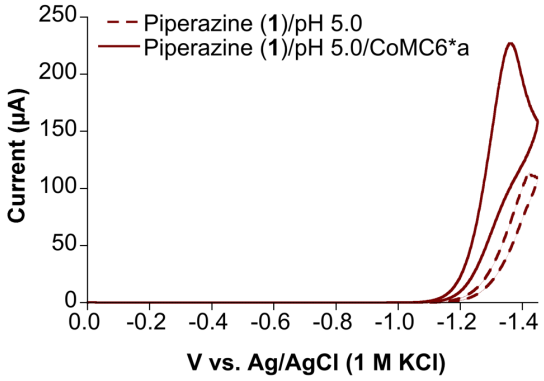

Figure S14. Cyclic voltammogram of CoMC6*a in 50 mM piperazine (**1**) at pH 5.0.

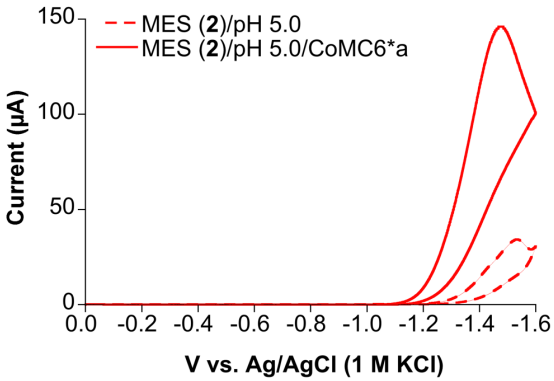

Figure S15. Cyclic voltammogram of CoMC6*a in 50 mM MES (**2**) at pH 5.0

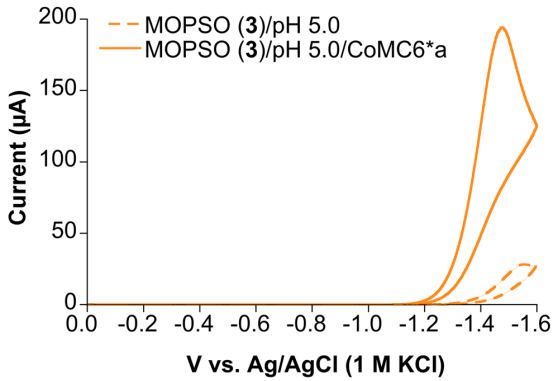

Figure S16. Cyclic voltammogram of CoMC6*a in 50 mM MOPSO (**3**) at pH 5.0

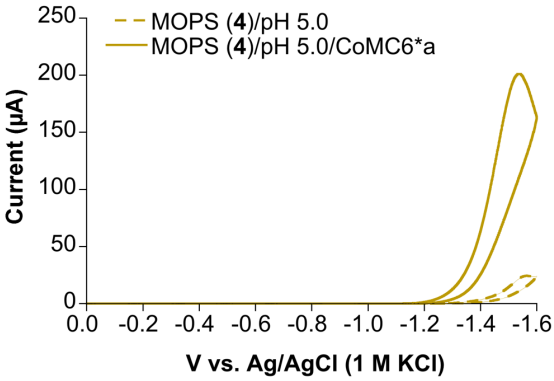

Figure S17. Cyclic voltammogram of CoMC6*a in 50 mM MOPS (**4**) at pH 5.0.

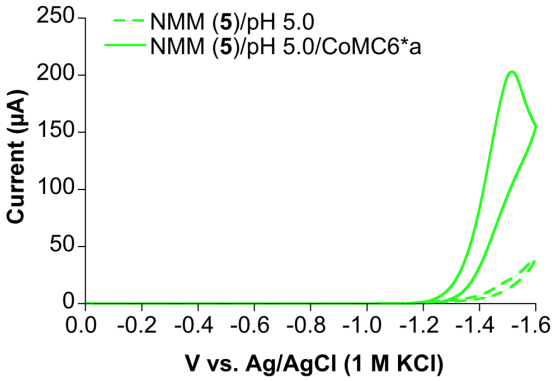

Figure S18. Cyclic voltammogram of CoMC6*a in 50 mM NMM (**5**) at pH 5.0.

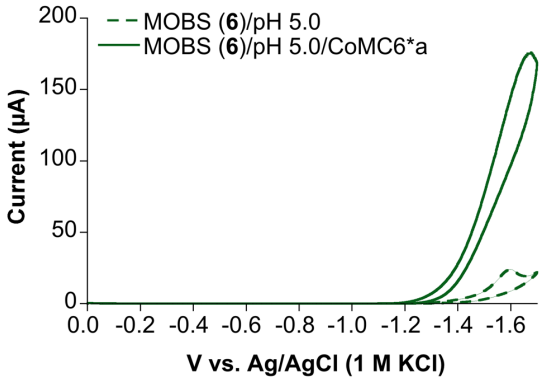

Figure S19. Cyclic voltammogram of CoMC6*a in 50 mM MOBS (**6**) at pH 5.0

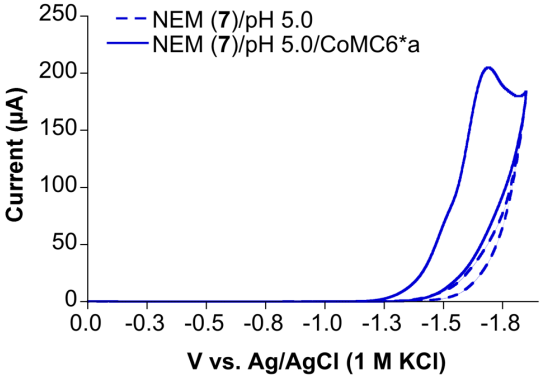

Figure S20. Cyclic voltammogram of CoMC6*a in 50 mM NEM (**7**) at pH 5.0.

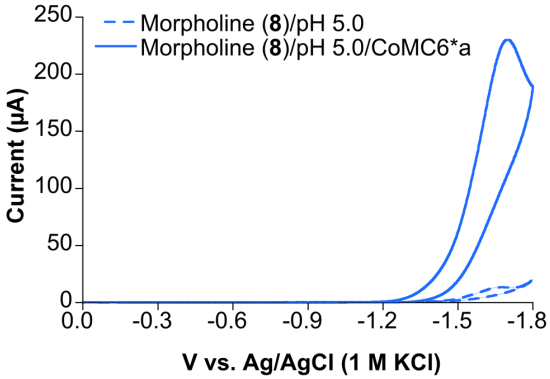

Figure S21. Cyclic voltammogram of CoMC6*a in 50 mM morpholine (**8**) at pH 5.0.

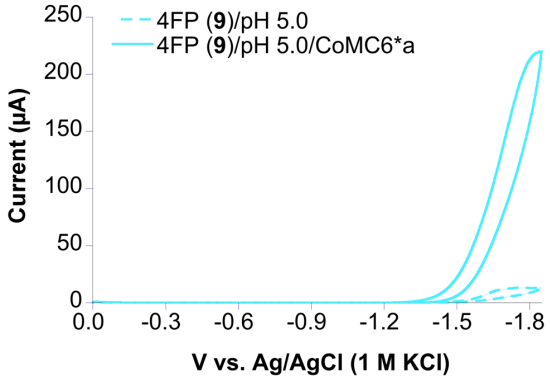

Figure S22. Cyclic voltammogram of CoMC6*a in 50 mM 4FP (**9**) at pH 5.0.

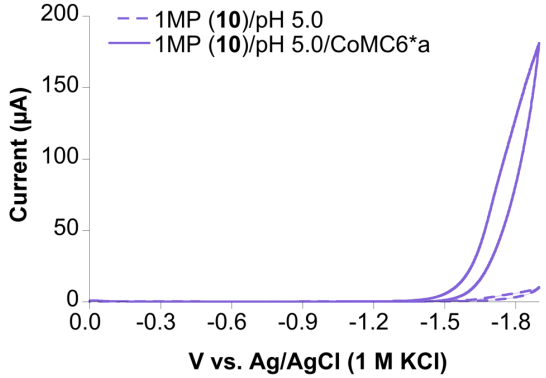

Figure S23. Cyclic voltammogram of CoMC6*a in 50 mM 1MP (**10**) at pH 5.0.

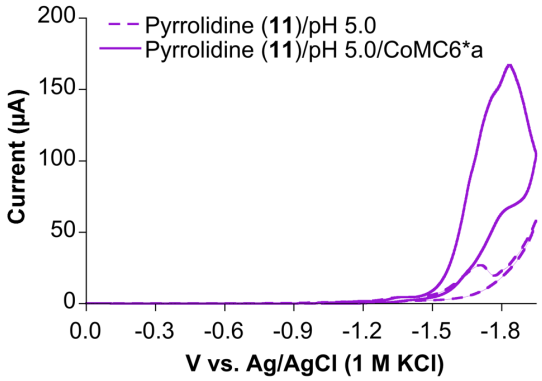

Figure S24. Cyclic voltammogram of CoMC6*a in 50 mM pyrrolidine (**11**) at pH 5.0.

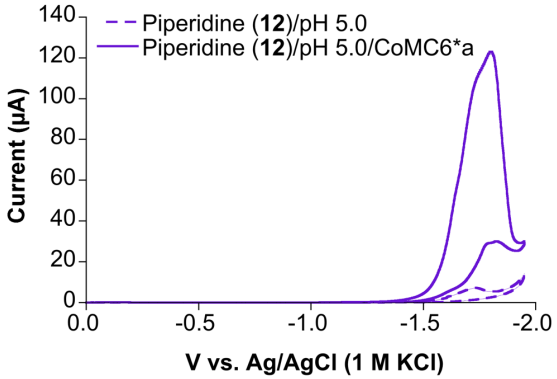

Figure S25. Cyclic voltammogram of CoMC6*a in 50 mM piperidine (**12**) at pH 5.0.

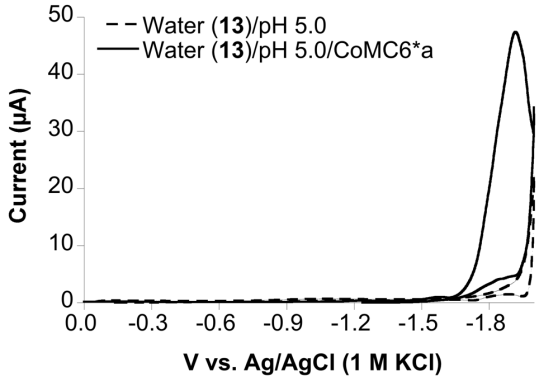

Figure S26. Cyclic voltammogram of CoMC6*a in water (**13**) at pH 5.0.

Table S2. E_h data from CVs that were collected under nitrogen at 100 mV/s scan rate with 1.0 μM CoMC6*a, 50 mM buffer, 100 mM KCl, and a pH of 5.0. A glassy carbon counter electrode, Ag/AgCl (1 M KCl) reference electrode, and HMDE working electrode were used. The E_h values are an average of three separate runs.

Buffer acid	pK_a	E_h (V vs. Ag/AgCl (1 M KCl)) ± STD DEV
1	5.8	–1.25 ± 0.03
2	6.1	–1.31 ± 0.01
3	6.9	–1.40 ± 0.01
4	7.1	–1.43 ± 0.01
5	7.4	–1.44 ± 0.01
6	7.5	–1.52 ± 0.02
7	7.7	–1.53 ± 0.02
8	8.7	–1.60 ± 0.04
9	9.4	–1.64 ± 0.01
10	10.3	–1.69 ± 0.02
11	11.5	–1.71 ± 0.01
12	11.6	–1.73 ± 0.01
13	14.0	–1.82 ± 0.01

*pK_a 1 is 5.8 for piperazine

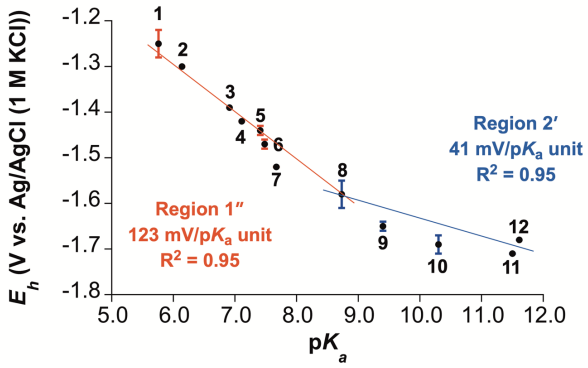

Figure S27. Plot of E_h values measured by CV for H_2 evolution by CoMC6*a as a function of proton donor pK_a for data collected at pH 5.0. Region 1 (solid red line) has a slope of –123 mV/pK_a unit, and region 2 (solid blue line) has a slope of –41 mV/pK_a unit. The red line (region 1) was fitted using E_h values from buffer acids **1**-**8**, and the blue line (region 2) was fitted using E_h values from buffer acids **8**-**12**. The CV data were collected under nitrogen at 100 mV/s scan rate with 1.0 μM CoMC6*a, 50 mM buffer, 100 mM KCl, and a pH of 5.0. A glassy carbon counter electrode, Ag/AgCl (1 M KCl) reference electrode, and HMDE working electrode were used. The E_h values are an average of three separate trials with standard deviation bars shown in the plot.

CVs of CoMC6*a in 1-4 at pH values one unit below the pK_a of 1-4

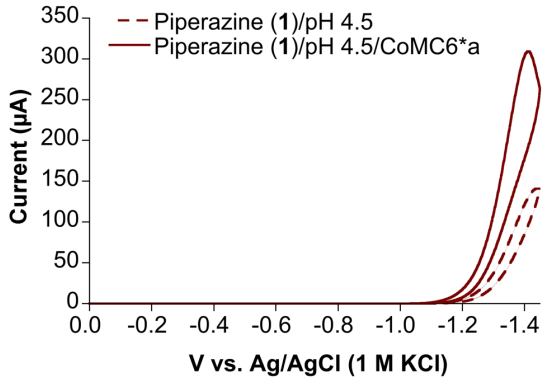

Figure S28. Cyclic voltammogram of CoMC6*a in 50 mM piperazine (**1**) at pH 4.5.

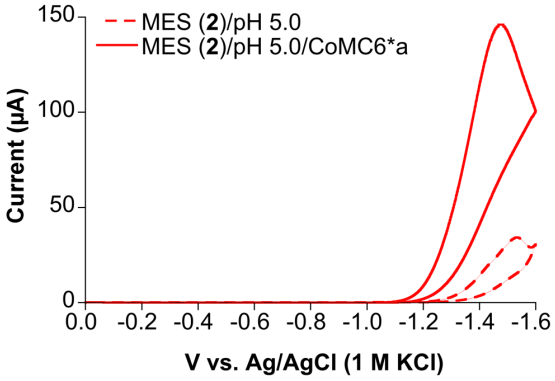

Figure S29. Cyclic voltammogram of CoMC6*a in 50 mM MES (**2**) at pH 5.0

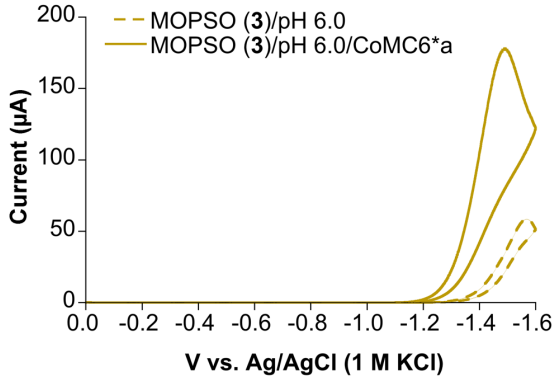

Figure S30. Cyclic voltammogram of CoMC6*a in 50 mM MOPSO (**3**) at pH 6.0.

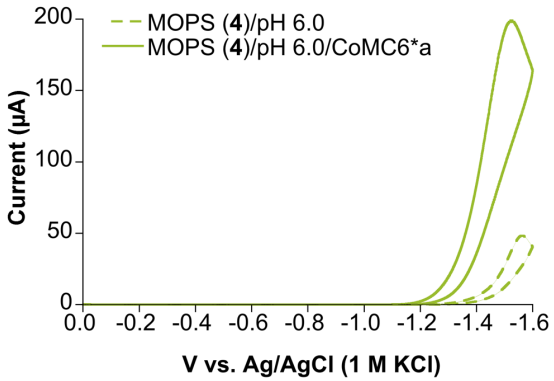

Figure S31. Cyclic voltammogram of CoMC6*a in 50 mM MOPS (**4**) at pH 6.0.

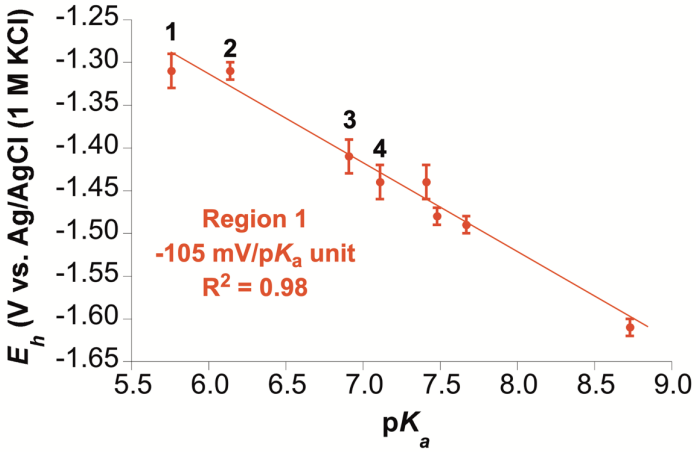

Figure S32. Plot of E_h values measured by CV for H_2 evolution by CoMC6*a as a function of buffer acid pK_a for data collected at a pH value 1 unit below each buffer pK_a. Region 1 (solid red line) has a slope of –105 mV/pK_a unit. CV data were collected under nitrogen at 100 mV/s scan rate with 1.0 µM CoMC6*a, 50 mM buffer acid, 100 mM KCl, and a pH of 4.5 for **1**, a pH of 5.0 for **2**, and pH values of 6.0 for **3** and **4**. A glassy carbon counter electrode, Ag/AgCl (1 M KCl) reference electrode, and HMDE working electrode were used. The E_h values are an average of three separate trials with standard deviation bars shown in the plot.

CVs of buffer acid titrations for 1-12

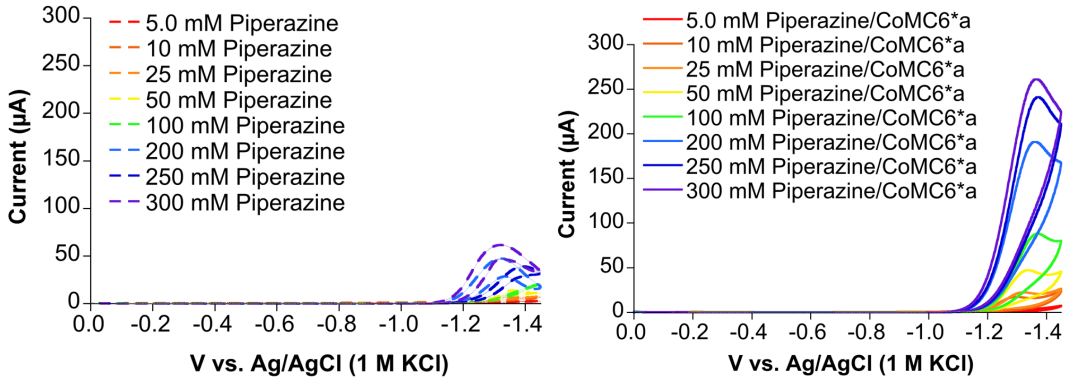

Figure S33. Left: Control CVs of varying piperazine concentration without CoMC6*a. Right: CVs of varying piperazine concentration from 5.0 to 300 mM with a constant concentration of 1.0 µM CoMC6*a.

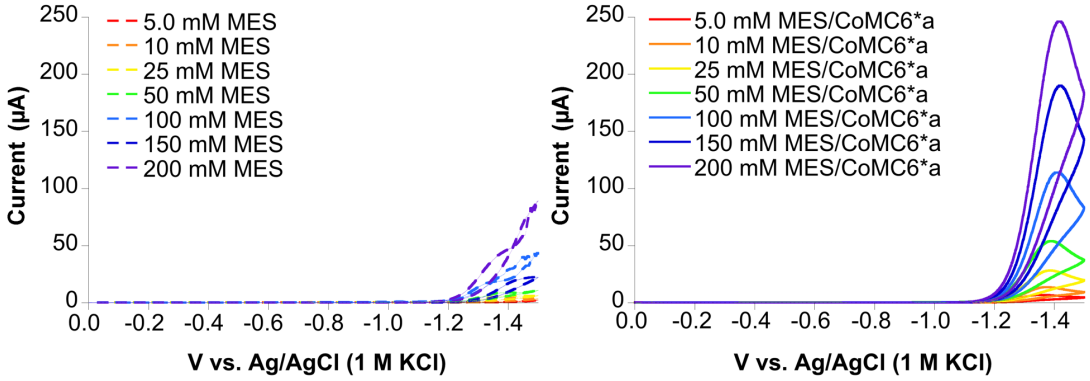

Figure S34. Left: Control CVs of varying MES concentration without CoMC6*a. Right: CVs of varying piperazine concentration from 5.0 to 200 mM with a constant concentration of 1.0 µM CoMC6*a.

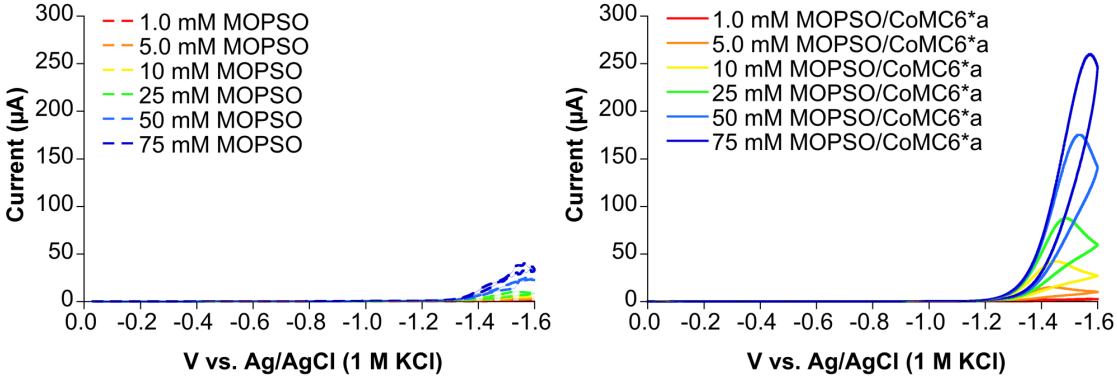

Figure S35. Left: Control CVs of varying MOPSO concentration without CoMC6*a. Right: CVs of varying MOPSO concentration from 5.0 to 75 mM with a constant concentration of 1.0 µM CoMC6*a.

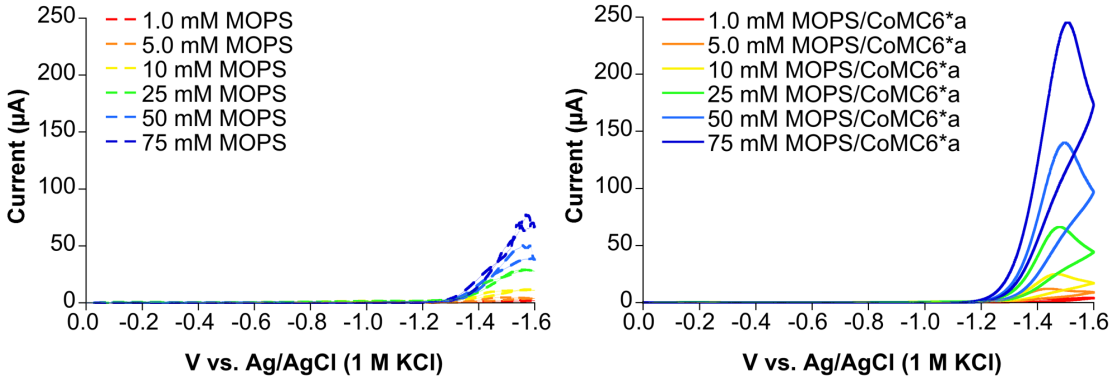

Figure S36. Left: Control CVs of varying MOPS concentration without CoMC6*a. Right: CVs of varying MOPS concentration from 5.0 to 75 mM with a constant concentration of 1.0 µM CoMC6*a.

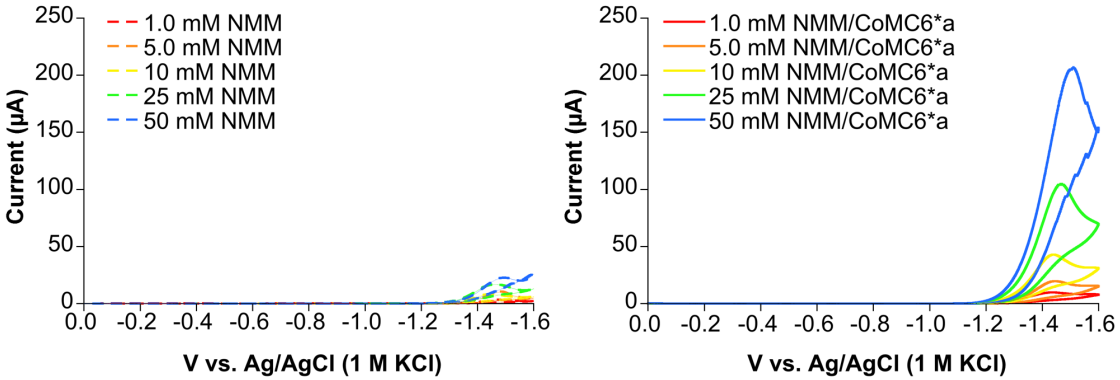

Figure S37. Left: Control CVs of varying NMM concentration without CoMC6*a. Right: CVs of varying NMM concentration from 1.0 to 50 mM with a constant concentration of 1.0 µM CoMC6*a.

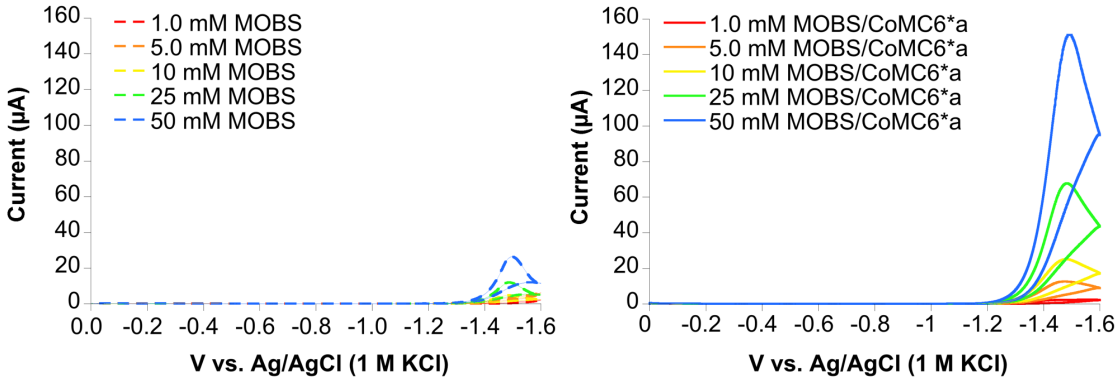

Figure S38. Left: Control CVs of varying MOBS concentration without CoMC6*a. Right: CVs of varying MOBS concentration from 1.0 to 50 mM with a constant concentration of 1.0 µM CoMC6*a.

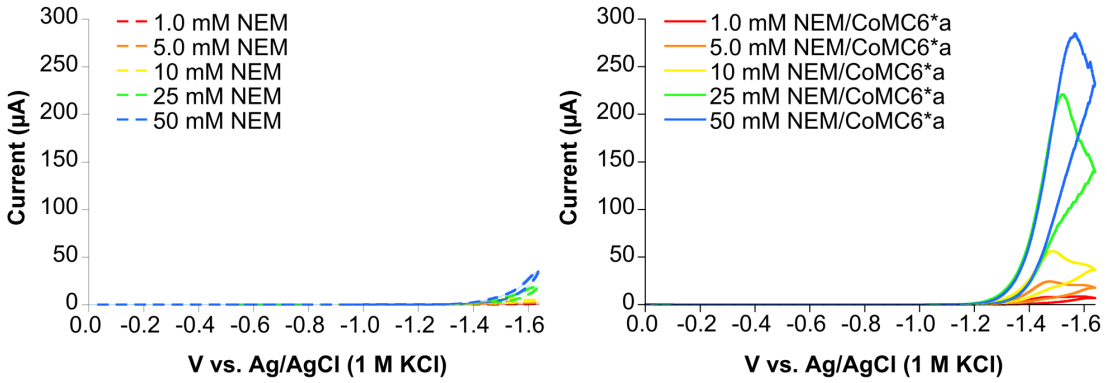

Figure S39. Left: Control CVs of varying NEM concentration without CoMC6*a. Right: CVs of varying NEM concentration from 1.0 to 50 mM with a constant concentration of 1.0 μM CoMC6*a.

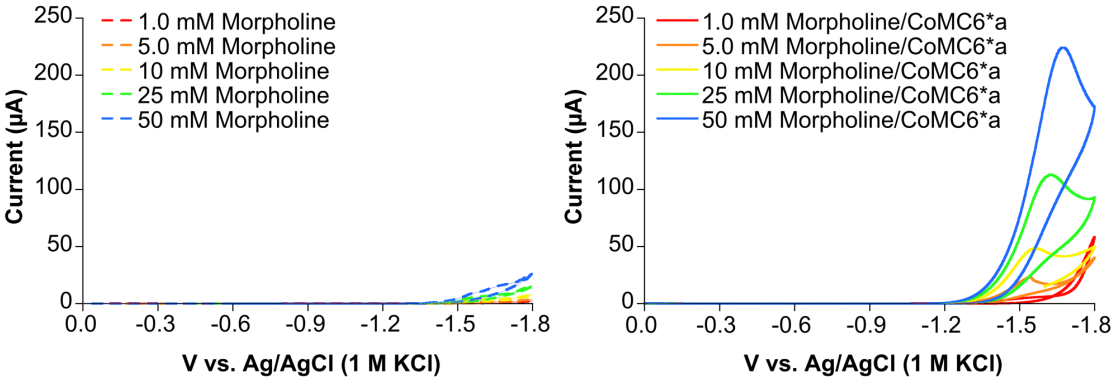

Figure S40. Left: Control CVs of varying morpholine concentration without CoMC6*a. Right: CVs of varying morpholine concentration from 1.0 to 50 mM with a constant concentration of 1.0 μM CoMC6*a.

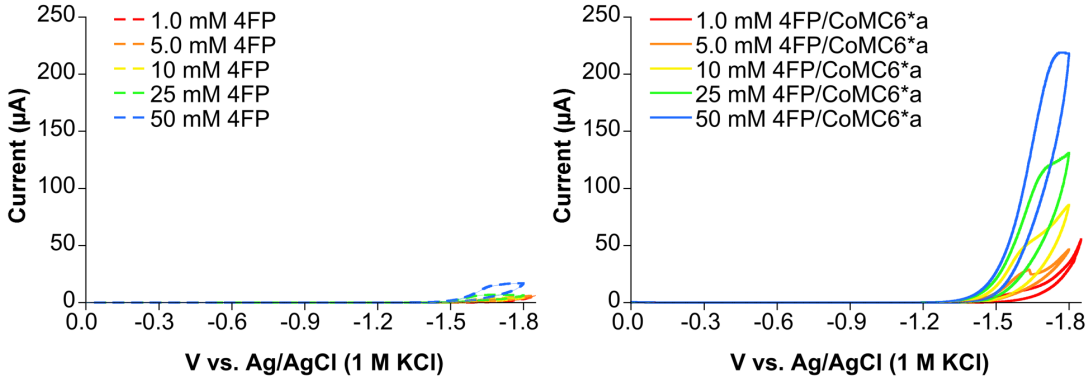

Figure S41. Left: Control CVs of varying 4FP concentration without CoMC6*a. Right: CVs of varying 4FP concentration from 1.0 to 50 mM with a constant concentration of 1.0 μM CoMC6*a.

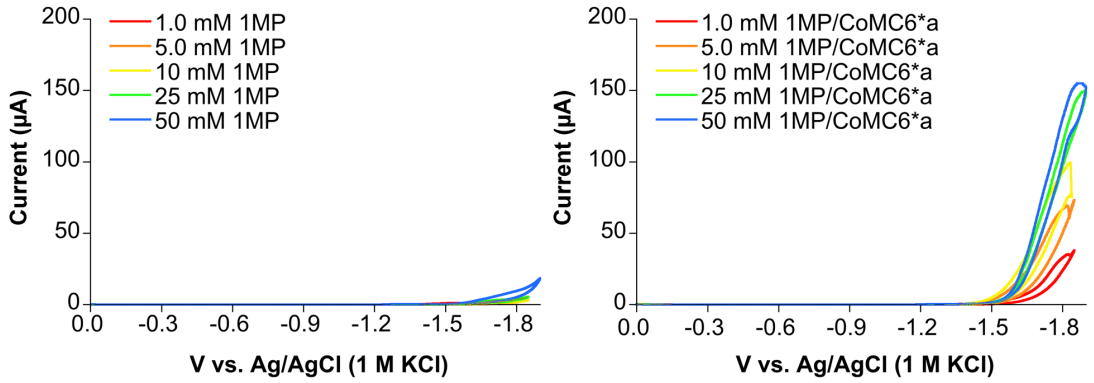

Figure S42. Left: Control CVs of varying 1MP concentration without CoMC6*a. Right: CVs of varying 1MP concentration from 1.0 to 50 mM with a constant concentration of 1.0 µM CoMC6*a.

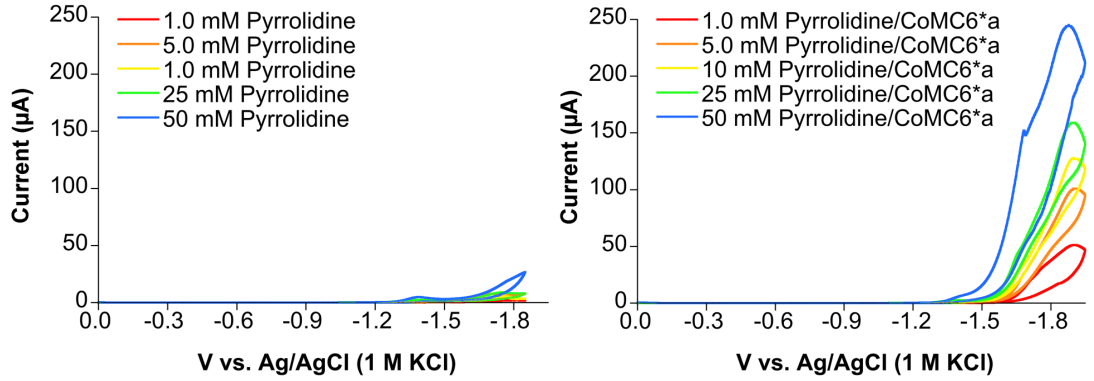

Figure S43. Left: Control CVs of varying pyrrolidine concentration without CoMC6*a. Right: CVs of varying pyrrolidine concentration from 1.0 to 50 mM with a constant concentration of 1.0 µM CoMC6*a.

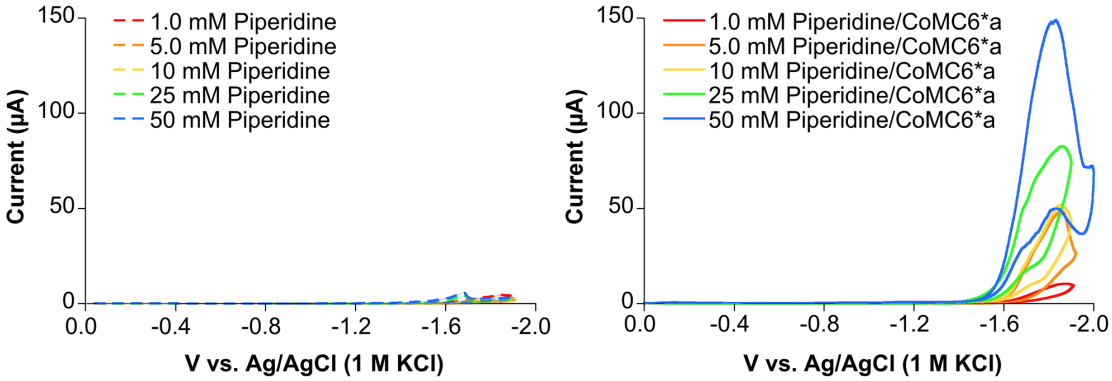

Figure S44. Left: Control CVs of varying piperidine concentration without CoMC6*a. Right: CVs of varying piperidine concentration from 1.0 to 50 mM with a constant concentration of 1.0 µM CoMC6*a.

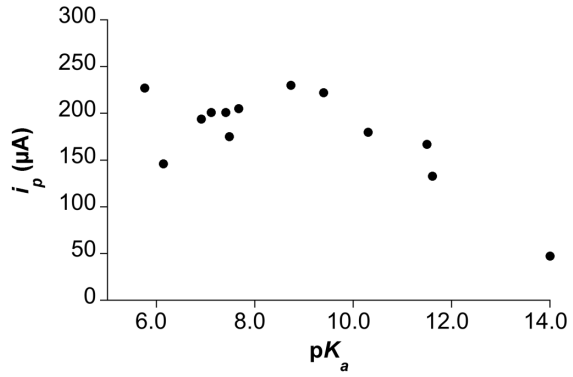

Figure S45. Plot of i_p vs. pK_a from CV data from Figs. S14-S26 of CoMC6*a in the presence of proton donors **1**-**13** at a constant pH of 5.0.

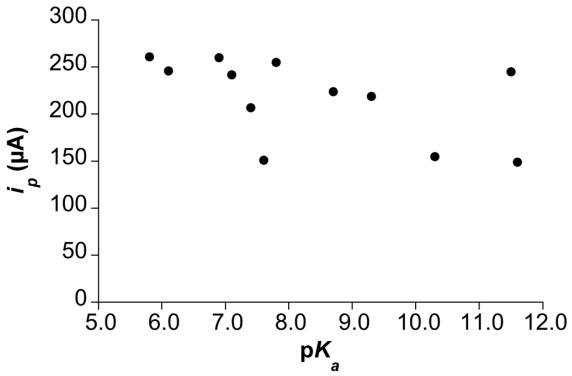

Figure S46. Plot of i_p vs. pK_a from CV data from Figs. S33-S44 of CoMC6*a in the presence of buffer acids **1**-**12** at a constant pH of 6.5 and constant concentration of the conjugate acid species at pH 6.5.

pK_a estimation of sterically hindered buffer acids by potentiometric titration

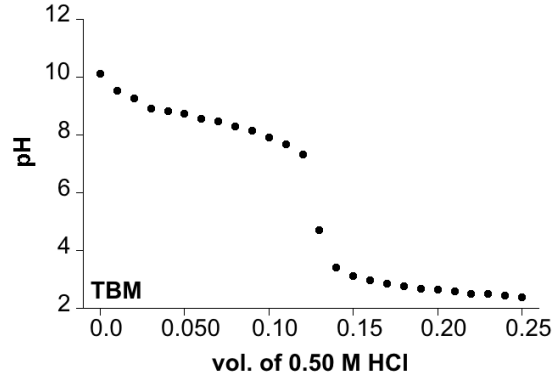

Figure S47. pK_a estimation of TBM by potentiometric titration. A concentration of 0.50 M HCl was titrated into 10 mL of 10 mM of TBM in increments of 10 µL. The solution was kept constantly stirring, and the pH was measured after reaching a steady pH reading. The estimated pK_a was 8.7.

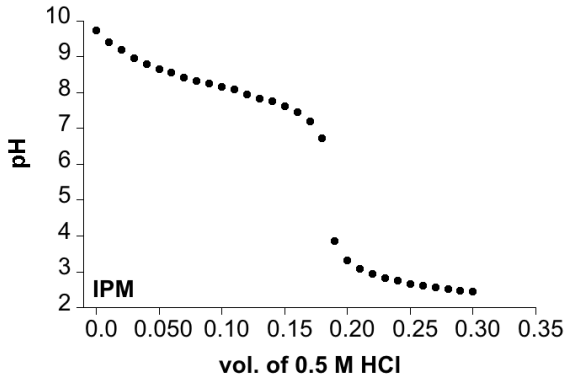

Figure S48. pK_a estimation of IPM by potentiometric titration. A concentration of 0.50 M HCl was titrated into 10 mL of 10 mM of IPM in increments of 10 µL. The solution was kept constantly stirring, and the pH was measured after reaching a steady pH reading. The estimated pK_a was 8.3.

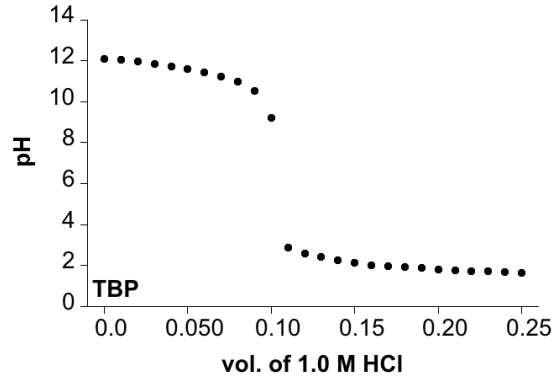

Figure S49. pK_a estimation of TBP by potentiometric titration. A concentration of 0.50 M HCl was titrated into 10 mL of 10 mM of TBP in increments of 10 µL. The solution was kept constantly stirring, and the pH was measured after reaching a steady pH reading. The estimated pK_a was 11.6.

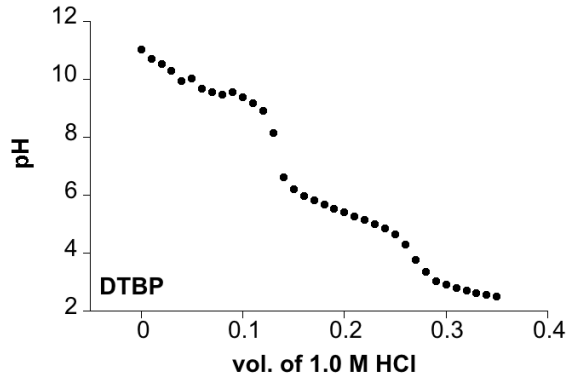

Figure S50. pK_a estimation of DTBP by potentiometric titration. A concentration of 1.0 M HCl was titrated into 10 mL of 25 mM of DTBP in increments of 10 µL. The solution was kept constantly stirring, and the pH was measured after reaching a steady pH reading. The estimated pK_a values were 5.3 (pK_a 1) and 9.6 (pK_a 2)

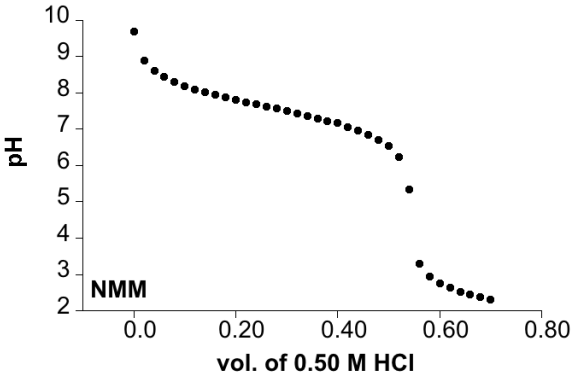

Figure S51. pK_a estimation of NMM by potentiometric titration. A concentration of 0.5 M HCl was titrated into 10 mL of 25 mM of NMM in increments of 20 µL. The solution was kept constantly stirring, and the pH was measured after reaching a steady pH reading. The estimated pK_a was 7.4, in agreement with literature value.[2]

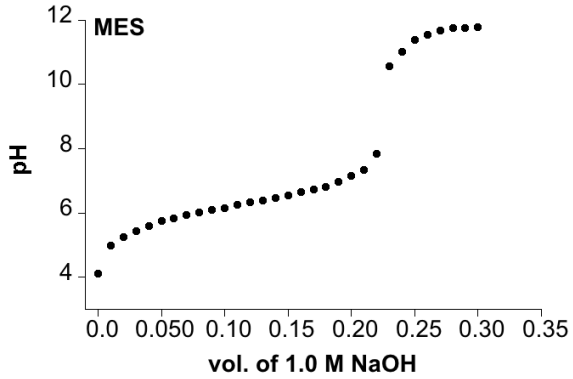

Figure S52. pK_a estimation of MES by potentiometric titration. A concentration of 1.0 M NaOH was titrated into 10 mL of 25 mM of MES in increments of 10 µL. The solution was kept constantly stirring, and the pH was measured after reaching a steady pH reading. The estimated pK_a was 6.1, in agreement with literature value.[2]

^{1}H-NMR and ^{13}C-NMR spectra

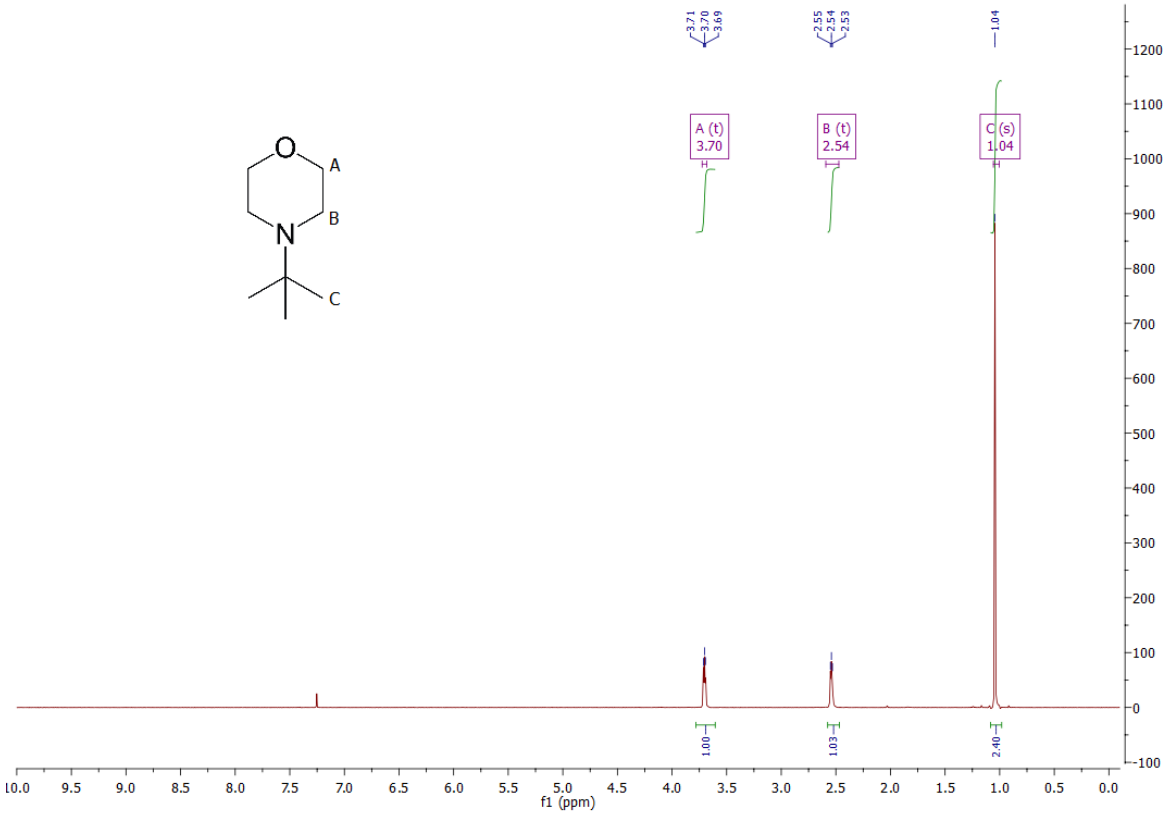

Figure S53. ^{1}H-NMR spectrum of TBM. ^{1}H-NMR of TBM in $CDCl_3$ was taken with a 400 MHz Bruker Avance instrument. Spectrum processed with MestReNova software. The spectrum matches with literature data.[3]

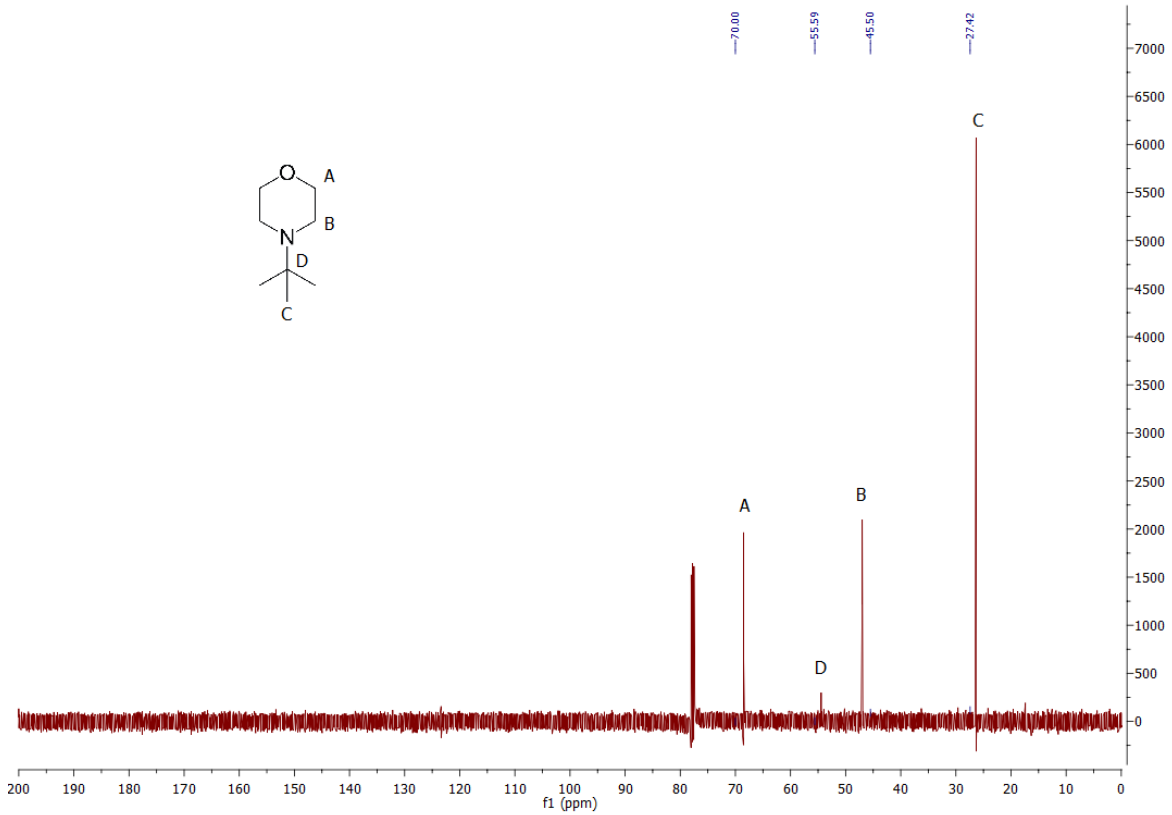

Figure S54. ^{13}C-NMR spectrum of TBM. ^{13}C-NMR of TBM in $CDCl_3$ was taken with a 400 MHz Bruker Avance instrument. Spectrum processed with MestReNova software. The spectrum matches with literature data.[4]

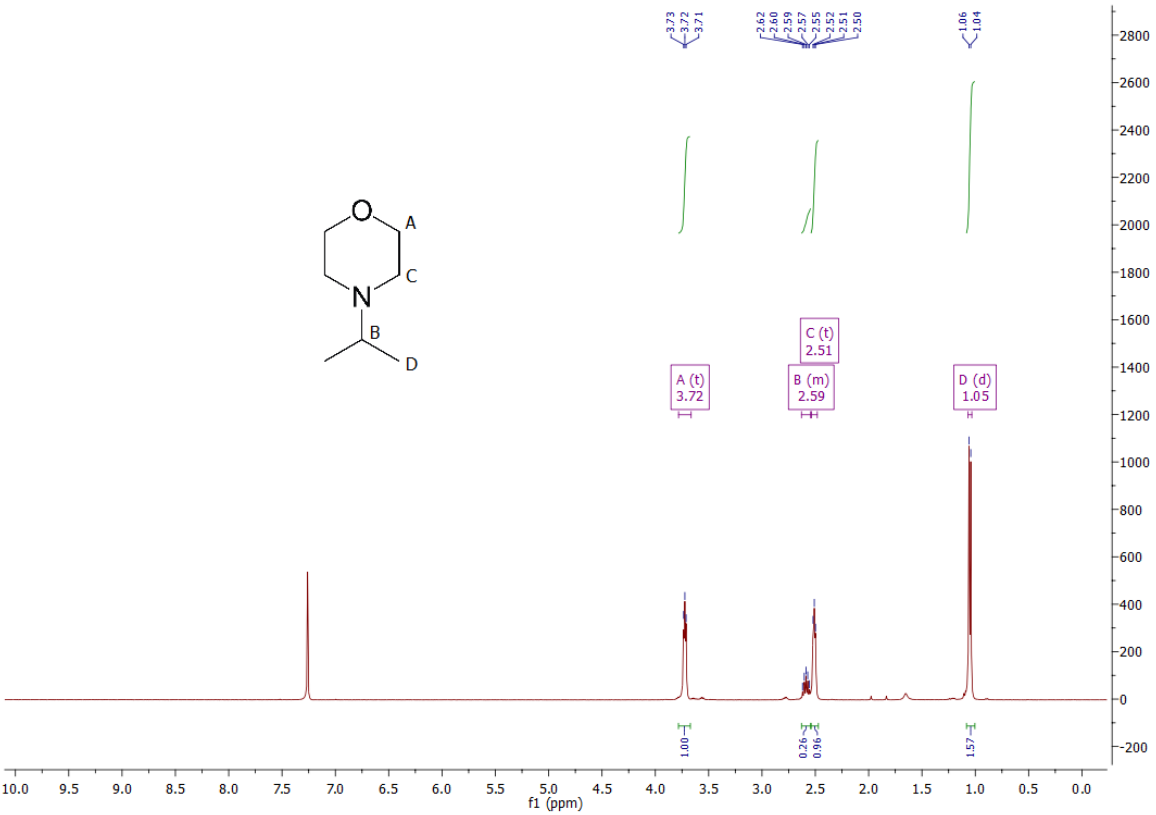

Figure S55. ^{1}H-NMR spectrum of IPM. ^{1}H-NMR of IPM in $CDCl_3$ was taken with a 400 MHz Bruker Avance instrument. Spectrum processed with MestReNova software. The spectrum matches with literature data.[5]

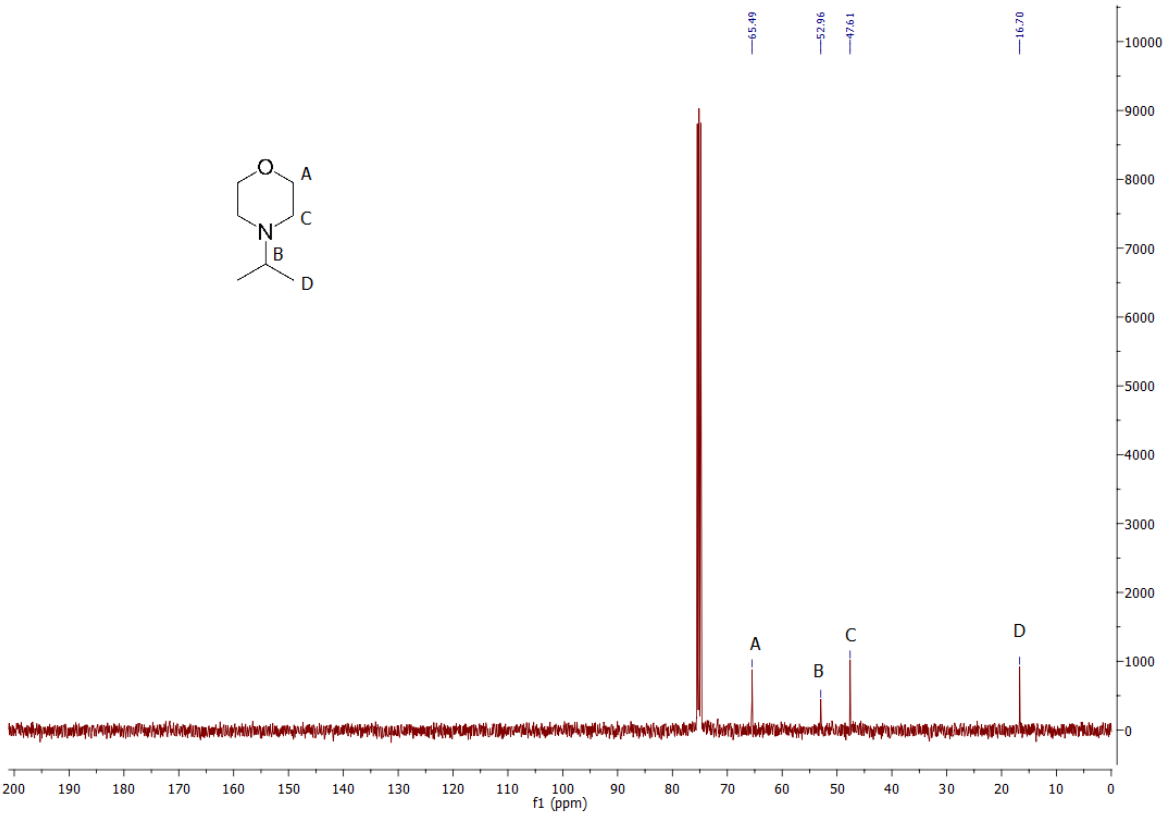

Figure S56. ^{13}C-NMR spectrum of IPM. ^{13}C-NMR of IPM in $CDCl_3$ was taken with a 400 MHz Bruker Avance instrument. Spectrum processed with MestReNova software. The spectrum matches with literature data.[5]

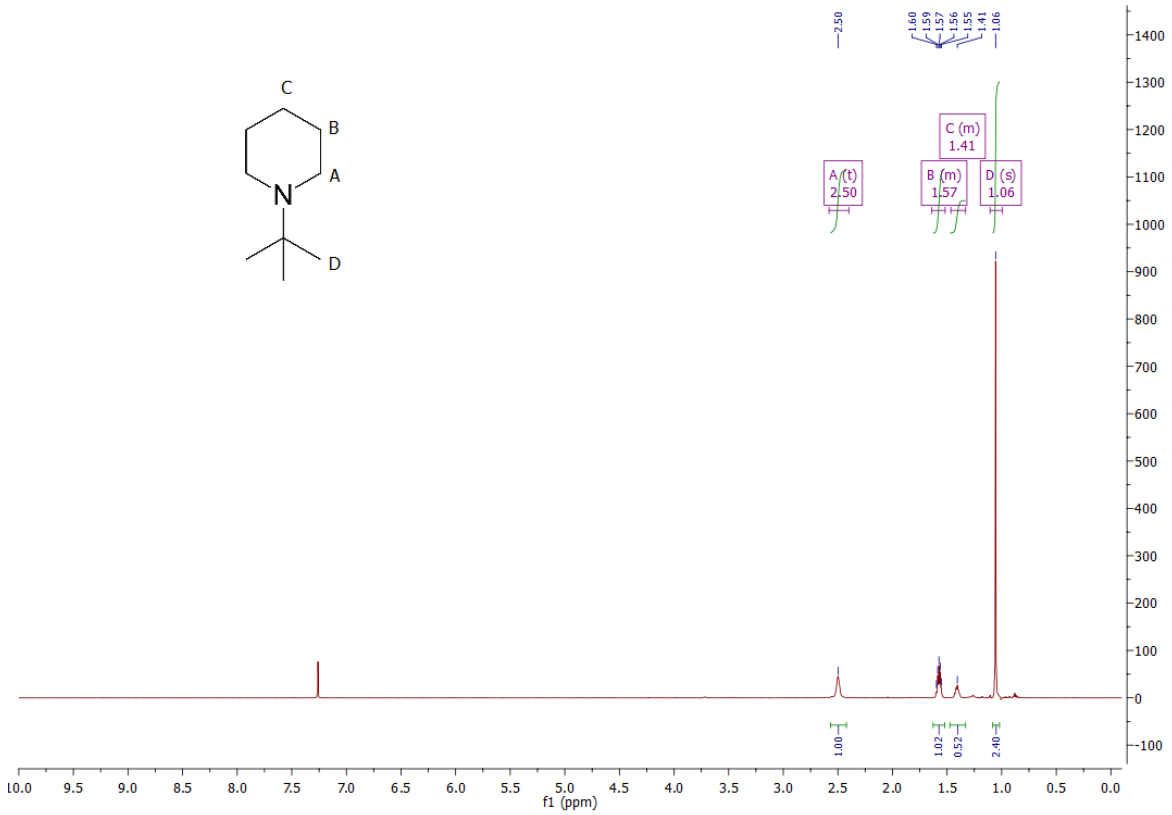

Figure S57. ^{1}H-NMR spectrum of TBP. ^{1}H-NMR of TBP in $CDCl_3$ was taken with a 400 MHz Bruker Avance instrument. Spectrum processed with MestReNova software. The spectrum matches with literature data.[6]

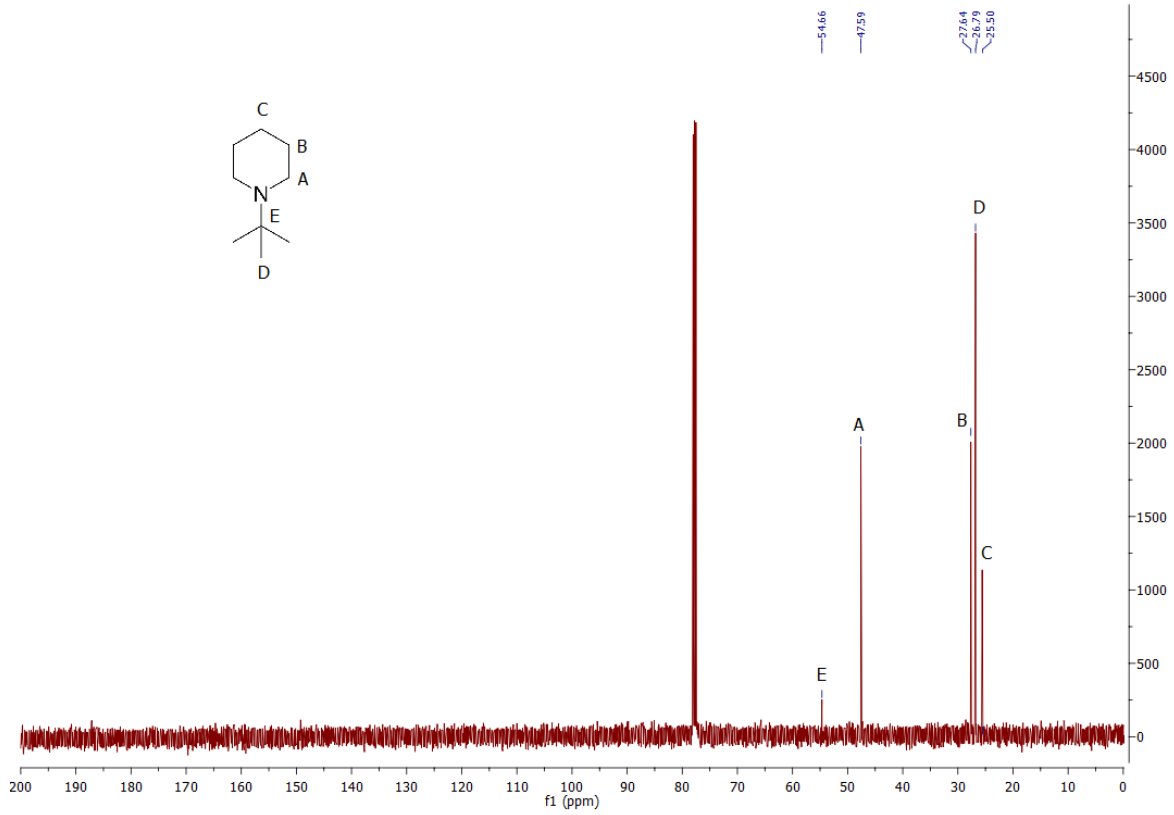

Figure S58. ^{13}C-NMR spectrum of TBP. ^{13}C-NMR of TBP in $CDCl_3$ was taken with a 400 MHz Bruker Avance instrument. Spectrum processed with MestReNova software. The spectrum matches with literature data.[7]

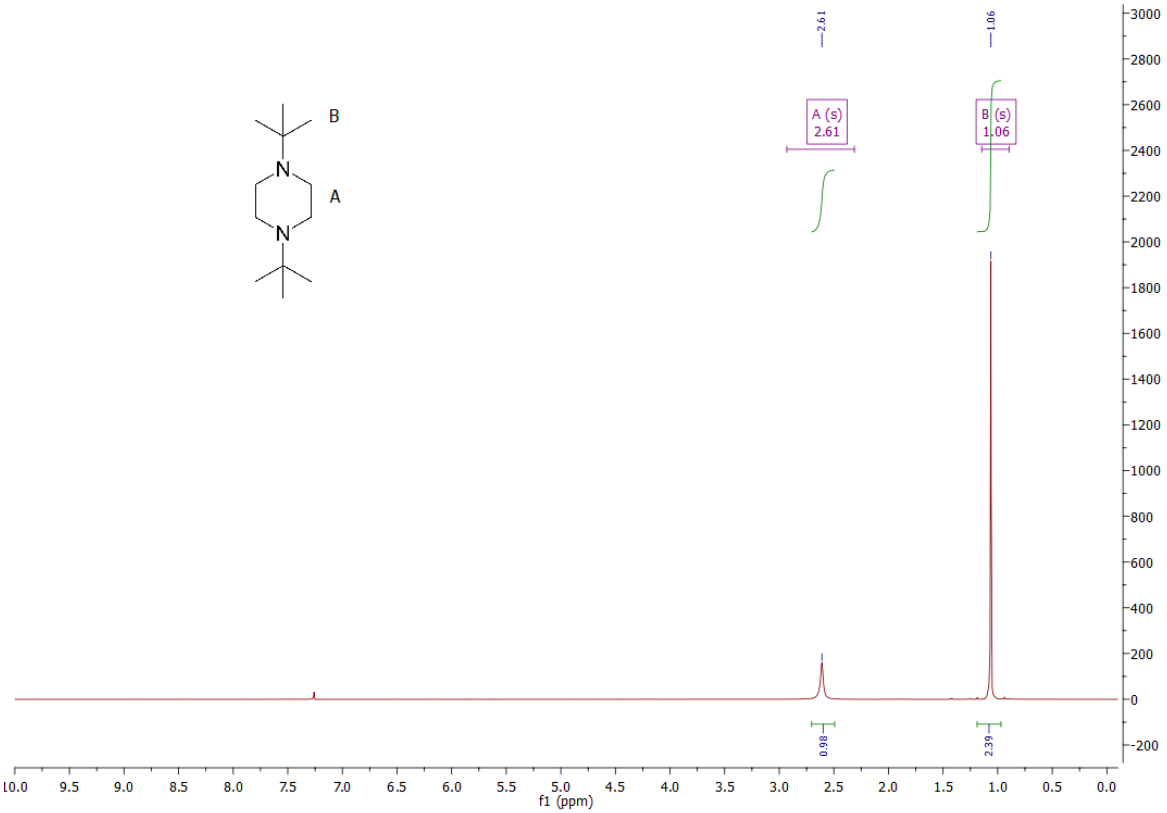

Figure S59. ^{1}H-NMR spectrum of DTBP. ^{1}H-NMR of DTBP in $CDCl_3$ was taken with a 500 MHz Bruker Avance instrument. Spectrum processed with MestReNova software. The spectrum matches with literature data.[6]

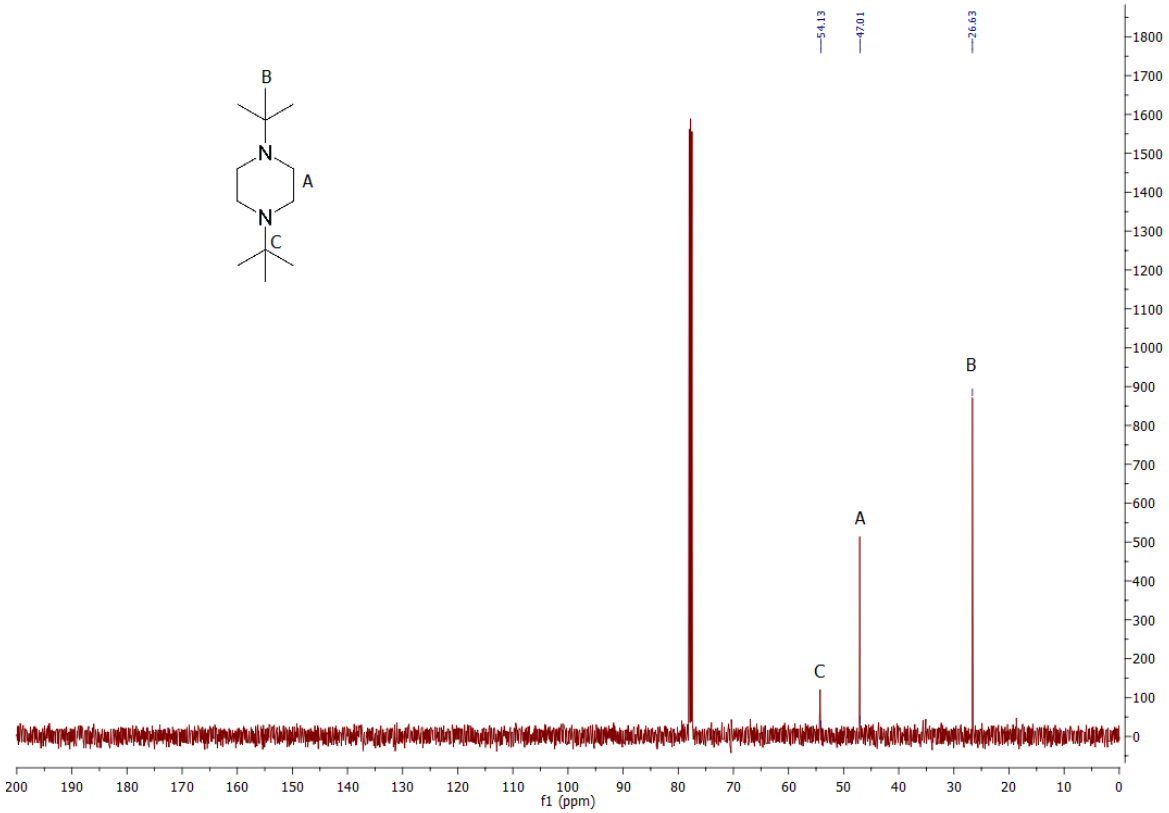

Figure S60. ^{13}C-NMR spectrum of DTBP. ^{13}C-NMR of DTBP in $CDCl_3$ was taken with a 500 MHz Bruker Avance instrument. Spectrum processed with MestReNova software. The spectrum matches with literature data.[8]

Table S3. Sterically hindered proton donors compared to their non-hindered derivatives. All E_h and i_p values are from CVs that were collected under nitrogen at 100 mV/s scan rate with 1.0 µM CoMC6*a, 50 mM buffer acid, 100 mM KCl, and a pH of 6.5. A glassy carbon counter electrode, Ag/AgCl (1 M KCl) reference electrode, and HMDE working electrode were used. The E_h values are an average of three separate runs with standard deviation values.

	Proton donor	pK_a	Avg E_h (V vs. Ag/AgCl (1 M KCl)) ± STD DEV	Avg i_p (µA)
1.	Piperazine	5.8	–1.23 ± 0.01	43 ± 12
1a.	DTBP	5.3	–1.27 ± 0.01	14 ± 6
8.	Morpholine	8.7	–1.61 ± 0.01	213 ± 8
8a.	IPM	8.3	–1.62 ± 0.00	72 ± 10
8b.	TBM	8.7	–1.63 ± 0.00	28 ± 4
12.	Piperidine	11.6	–1.73 ± 0.01	158 ± 17
12a.	TBP	11.6	–1.80 ± 0.02	81 ± 20

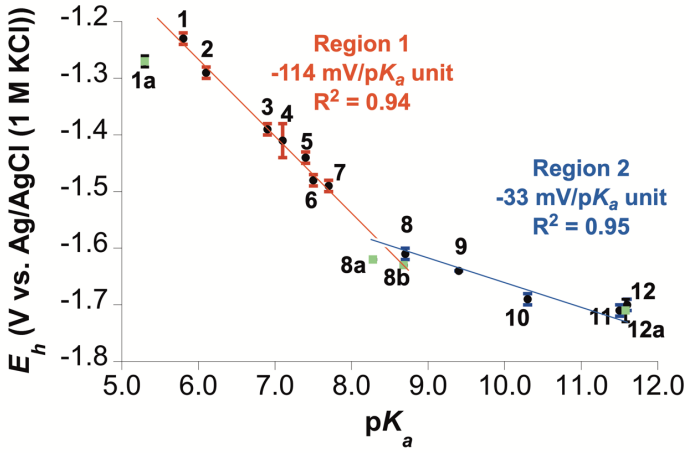

Figure S61. The plot of E_h values measured by CV for H_2 evolution by CoMC6*a as a function of buffer acid pK_a including sterically hindered proton donors (green squares). Region 1 (solid red line) has a slope of –122 mV/pK_a unit, and region 2 has a slope of –37 mV/pK_a unit. The red line (region 1) was fitted using E_h values from proton donors **1**-**8** and **8a**-**b**. The blue line (region 2) was fitted using E_h values from proton donors **8-12**, **8a**-**b**, and **12a**. CV data were collected under nitrogen at 100 mV/s scan rate with 1.0 μM CoMC6*a, 50 mM proton donor, 100 mM KCl, and a pH of 6.5. A glassy carbon counter electrode, Ag/AgCl (1 M KCl) reference electrode, and HMDE working electrode were used. The E_h values are an average of three separate trials with standard deviation bars shown in the plot.

CVs of sterically hindered proton donors without CoMC6*a at pH 6.5

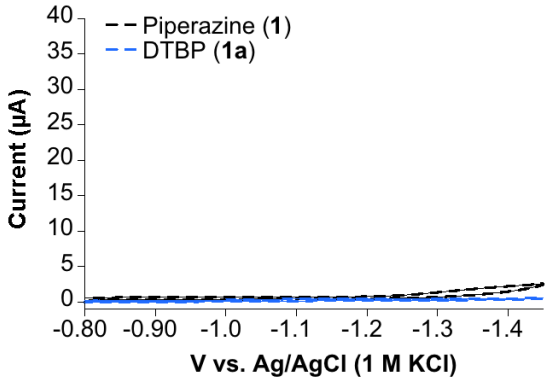

Figure S62. Control CVs of 50 mM piperazine (**1**, black) and 50 mM DTBP (**1a**, blue) without CoMC6*a.

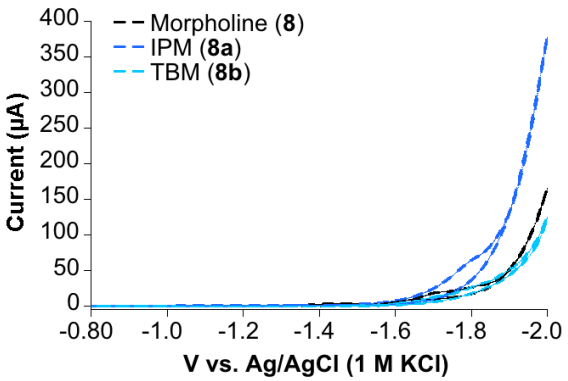

Figure S63. Control CVs of 50 mM morpholine (**8**, black), 50 mM IPM (**8a**, blue), and 50 mM TBM (**8b**, light blue) without CoMC6*a.

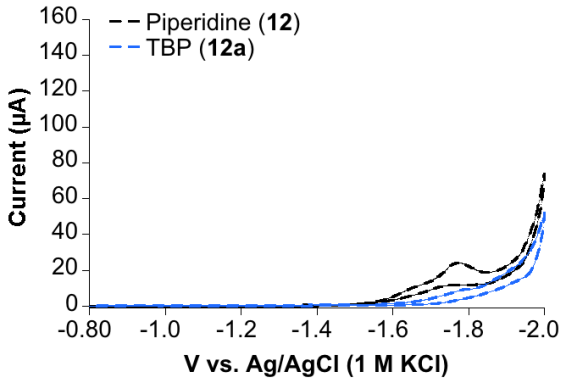

Figure S64. Control CVs of 50 mM piperidine (**12**, black) and 50 mM TBP (**12a**, blue) without CoMC6*a.

The following equation was used to calculate the overpotential for the Co(II/I) reduction potential of the cobalt bis(aminopyridine complex),[1] where 244 mV is the conversion from the SCE reference electrode to the SHE reference electrode, and the 414 mV is the oxidation potential vs. SHE of the H+/H_2 couple at pH 7.0:

Overpotential = |Co(II/I) reduction potential reported in ref. 8 + 244 mV + 414 mV| [**S1**]

The following equation was used to calculate overpotential for the possible Co(II/I) potential of CoMC6*a based on the E_h value of –1.82 V, where 235 mV is the conversion from the Ag/AgCl (1 M KCl) reference electrode to the SHE reference electrode, and 385 mV is the oxidation potential vs. SHE of the H+/H_2 couple at pH 6.5:

Overpotential = |half-wave potential + 235 mV + 385 mV| [**S2**]

Syntheses of sterically hindered proton donors

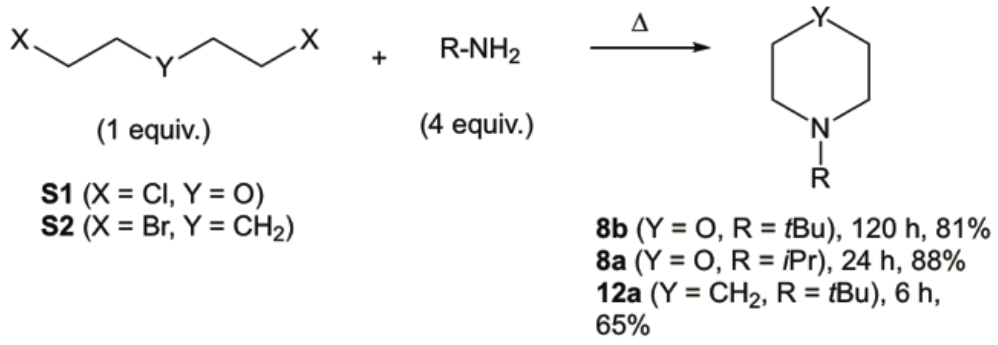

Scheme S1. Synthesis of TBM (**8b**), IPM (**8a**), TBP (**12a**).

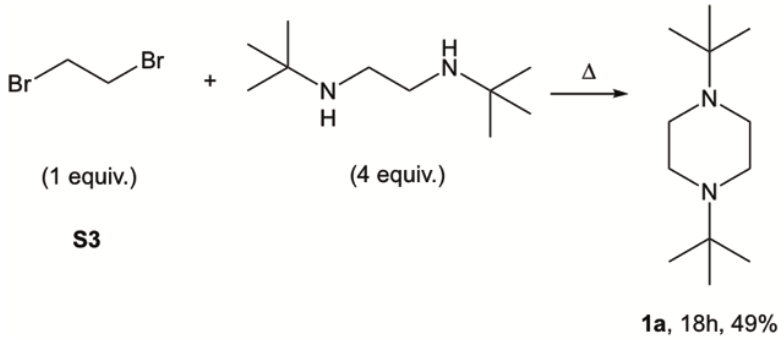

Scheme S2. Synthesis of DTBP (**1a**).

References

(1) Stubbert, B. D.; Peters, J. C.; Gray, H. B. Rapid Water Reduction to H 2 Catalyzed by a Cobalt Bis(Iminopyridine) Complex. *J. Am. Chem. Soc.* **2011**, *133* (45), 18070–18073. https://doi.org/10.1021/ja2078015.

(2) *CRC Handbook of Chemistry and Physics, 92nd Edition*; CRC Press, 2011. https://doi.org/10.1201/b17379.

(3) Carpino, L. A.; Ionescu, D.; El-Faham, A. Peptide Coupling in the Presence of Highly Hindered Tertiary Amines. *J. Org. Chem.* **1996**, *61* (7), 2460–2465. https://doi.org/10.1021/jo950912x.

(4) Walker, W. K.; Anderson, D. L.; Stokes, R. W.; Smith, S. J.; Michaelis, D. J. Allylic Aminations with Hindered Secondary Amine Nucleophiles Catalyzed by Heterobimetallic Pd–Ti Complexes. *Org. Lett.* **2015**, *17* (3), 752–755. https://doi.org/10.1021/acs.orglett.5b00058.

(5) Suzuki, K.; Okano, K.; Nakai, K.; Terao, Y.; Sekiya, M. Reductive Rearrangement of 2-Chloroalkanamides with Lithium Aluminum Hydride Leading to α-Methyl-Branched Aliphatic Amines. *Synthesis (Stuttg).* **1983**, *1983* (09), 723–725. https://doi.org/10.1055/s-1983-30487.

(6) Salamone, M.; Martella, R.; Bietti, M. Hydrogen Abstraction from Cyclic Amines by the Cumyloxyl and Benzyloxyl Radicals. The Role of Stereoelectronic Effects and of Substrate/Radical Hydrogen Bonding. *J. Org. Chem.* **2012**, *77* (19), 8556–8561. https://doi.org/10.1021/jo3015352.

(7) Al-Rawi, J. M. A.; Flamerz, S.; Khuthier, A. H. 13C Nuclear Magnetic Resonance Spectra of Some N-Alkylpiperidines and the Corresponding N-Oxides. N-Substitution and N-Oxidation Effects. *Spectrochim. Acta Part A Mol. Spectrosc.* **1985**, *41* (12), 1391–1395. https://doi.org/10.1016/0584-8539(85)80192-6.

(8) Denk, M. K.; Krause, M. J.; Niyogi, D. F.; Gill, N. K. Reaction of 1,2-Dibromoethane with Primary Amines: Formation of N , N ′-Disubstituted Ethylenediamines RNH–CH 2 CH 2 –NHR and Homologous Polyamines RNH–[CH 2 CH 2 NR] n –H. *Tetrahedron* **2003**, *59* (38), 7565–7570. https://doi.org/10.1016/S0040-4020(03)01149-9.